

# The Physics of DAΦNE and KLOE

PAOLO FRANZINI

*Dipartimento di Fisica dell'Università di Roma, La Sapienza e Sezione dell'Istituto Nazionale di Fisica Nucleare, Roma, Italy; email: Paolo.Franzini@lnf.infn.it*

MATTHEW MOULSON

*Laboratori Nazionali di Frascati dell'Istituto Nazionale di Fisica Nucleare, Frascati, Italy; email: Matthew.Moulson@lnf.infn.it*

**Key Words** *CP violation, CKM matrix, muon anomalous magnetic moment, exotic atoms, hypernuclei*

**Abstract** DAΦNE, the Frascati  $\phi$  factory, has been in operation since 1999. At the center of the physics program is the KLOE experiment, a multipurpose detector with optimizations for tagged and interferometry-based measurements of the neutral kaon system. KLOE has been taking data since 2000 and has helped to explore a wide array of topics in kaon and hadronic physics, including a comprehensive set of measurements to determine the CKM matrix element  $|V_{us}|$ , and a measurement of the  $e^+e^- \rightarrow \pi^+\pi^-$  cross section for the determination of the hadronic contribution to the muon anomaly. In addition, the DEAR experiment has measured the X-ray spectrum of kaonic hydrogen, and the FINUDA experiment has conducted its first studies in hypernuclear spectroscopy and a search for  $\bar{K}$ -nuclear bound states. We review the design, construction, and operation of the DAΦNE facility, with an emphasis on the physics program of the KLOE experiment.

## Contents

INTRODUCTION . . . . .	2
DAΦNE: THE FRASCATI $\phi$ FACTORY . . . . .	3
THE KLOE EXPERIMENT . . . . .	4
KAON PHYSICS . . . . .	7
<i>Why a <math>\phi</math> Factory?</i> . . . . .	7
<i><math>K_L</math> Decays</i> . . . . .	10
<i><math>K_S</math> Decays</i> . . . . .	14
<i>Charged Kaon Decays</i> . . . . .	17
<i>KLOE, <math>V_{us}</math>, and CKM Unitarity</i> . . . . .	20
HADRONIC PHYSICS . . . . .	21
<i>Pseudoscalar Mesons: <math>\eta</math> and <math>\eta'</math></i> . . . . .	21
<i>Scalar Mesons: <math>f_0(980)</math> and <math>a_0(980)</math></i> . . . . .	23
<i>The Hadronic Cross Section and <math>a_\mu</math></i> . . . . .	26
THE DEAR AND SIDDHARTA EXPERIMENTS . . . . .	29

<i>Kaonic Atoms and the <math>\bar{K}N</math> Interaction</i> . . . . .	29
<i>Measurement of the X-Ray Spectrum of Kaonic Hydrogen</i> . . . . .	30
<b>FINUDA</b> . . . . .	32
<i>Hypernuclear Physics at a <math>\phi</math> Factory</i> . . . . .	32
<i>First Results from the FINUDA Experiment</i> . . . . .	33
<b>THE FUTURE OF DAΦNE</b> . . . . .	35

## 1 INTRODUCTION

The experimental study of kaon decays has played a singular role in propelling the development of particle physics for nearly 60 years. Of particular importance, the 1963 observation at Brookhaven National Laboratory of the decay  $K_L \rightarrow \pi^+\pi^-$  (1) was the first experimental evidence of  $CP$  violation in any physical system. For more than 50 years, the question remained of whether  $CP$  violation was confined to the  $|\Delta S| = 2$   $K^0 \rightleftharpoons \bar{K}^0$  transition, resulting in a small  $CP$  impurity in the neutral kaon mass eigenstates, or whether  $CP$  is also violated directly, i.e., in the  $|\Delta S| = 1$  kaon decay amplitudes. The former possibility, often referred to as the superweak hypothesis (2), remained viable until quite recently. From 1988–1992, the first hints of direct  $CP$  violation were observed (3). It soon became clear, however, that to definitively establish its existence would require increased sensitivity.

The search for direct  $CP$  violation was the major impetus for the construction in Frascati of an  $e^+e^-$  collider to operate at a center-of-mass energy equal to the mass of the  $\phi$  meson. In 1990 the Istituto Nazionale di Fisica Nucleare approved the proposal (4) for the collider, named DAΦNE (Double Annular  $\Phi$  factory for Nice Experiments). The DAΦNE luminosity goal was  $5 \times 10^{32} \text{ cm}^{-2} \text{ s}^{-1}$ ; that is, DAΦNE was to produce  $\sim 1300$  kaon pairs per second, or  $\sim 4 \times 10^{10}$  pairs per year at 100% efficiency.

A first-round search for direct  $CP$  violation at DAΦNE would require an integrated luminosity of  $\sim 10 \text{ fb}^{-1}$ . The physics program was to be complemented by other topics. The KLOE experiment (5), named after Chloë, the literary counterpart to Daphnis, was proposed in 1992 to carry out an ambitious and wide-ranging program in neutral kaon physics (using especially  $K_S K_L$  interferometry), charged kaon physics, and measurements of the properties of scalar and pseudoscalar mesons. The precise determinations of  $\phi$  and  $K$  meson properties—masses, leptonic widths, branching ratios (BRs), and lifetimes—were central to this program. In particular, the partial widths for leptonic and semileptonic kaon decays are fundamental parameters for comparison with Standard Model predictions. Another important element of the program was the measurement of the hadronic cross section, especially for  $e^+e^- \rightarrow \pi^+\pi^-$ , which is needed to calculate the hadronic contribution to the photon spectral function in computing the muon anomaly,  $(g_\mu - 2)/2$ .

Two additional experiments were subsequently proposed to capitalize on the availability of low-energy charged kaons at the second DAΦNE interaction point: FINUDA (Fisica Nucleare a DAΦNE) (6) in 1993 for the study of hypernuclear spectroscopy, and DEAR (DAΦNE Exotic Atom Research) (7) in 1995 for the spectroscopy of  $K$ -mesic hydrogen atoms.

In 2005, the DAΦNE luminosity reached  $1.3 \times 10^{32} \text{ cm}^{-2} \text{ s}^{-1}$ . An integrated luminosity of  $\sim 2.5 \text{ fb}^{-1}$  was delivered to KLOE between 1999 and 2005. Although far smaller than necessary for a competitive search for direct  $CP$  violation, this data set has permitted KLOE to explore the breadth of its original physics agenda. KLOE has performed measurements of the partial decay rates for kaons fundamental to the study of quark mixing,

has vastly improved experimental knowledge of scalar and pseudoscalar meson states, and has completed a first round of measurements of  $\sigma(e^+e^- \rightarrow \text{hadrons})$ . In addition, DEAR has measured the level shifts and widths of kaonic hydrogen, and FINUDA has obtained first results on hypernuclear spectroscopy and conducted a search for new states from nuclear  $K^-$  absorption.

## 2 DAΦNE: THE FRASCATI $\phi$ FACTORY

DAΦNE, like PEP-II at the Stanford Linear Accelerator Center and KEKB at the KEK laboratory in Japan, uses two separate rings to store large numbers of electron and positron bunches, thus avoiding beam-beam interaction effects. The DAΦNE design parameters—a luminosity goal of  $5 \times 10^{32} \text{ cm}^{-2} \text{ s}^{-1}$  in 120-bunch operation in a machine with rings 98 m in circumference—imply a stored current of approximately 5 A in each beam. The beams intersect at an angle of  $(\pi - 0.025)$  rad in two interaction regions (IRs) on opposite sides of the rings, where low- $\beta$  insertions provide focusing to obtain high luminosity (8). At the IRs, the bunches are flat in cross section, with  $\sigma_x \approx 2 \text{ mm}$  and  $\sigma_y \approx 10 \text{ } \mu\text{m}$ . Figure 1 shows a plan view of the DAΦNE complex.

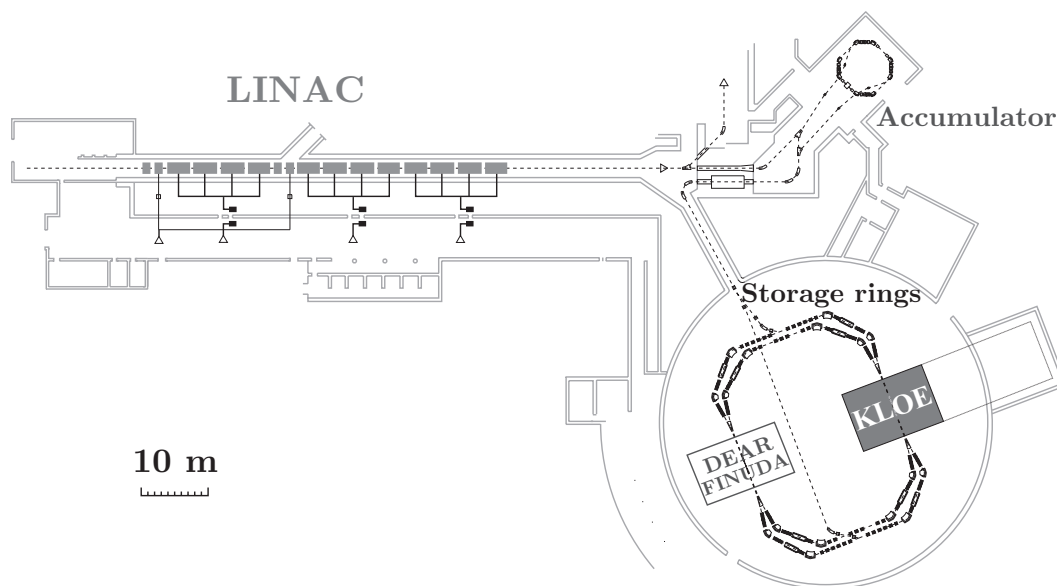


**Fig. 1.** Schematic diagram of the DAΦNE facility.

A two-stage linac produces electrons and positrons of 510 MeV, with a repetition rate of 50 Hz. These are stacked and cooled in the accumulator ring. Bunches are transferred from the accumulator to the DAΦNE rings on-energy at a rate of 1 Hz. Each DAΦNE ring consists of four bending sections, each with a wiggler magnet, and a large number of quadrupoles to provide the basic alternating-gradient focusing structure. The four wigglers in each ring help to reduce the damping times for synchrotron and betatron oscillations, which still remain  $\sim 50,000$  times larger than the cyclotron period.

DAΦNE operations got off to a rough start. The highest luminosity sustained during the year following KLOE roll-in in April 1999 was  $\sim 2 \times 10^{30} \text{ cm}^{-2} \text{ s}^{-1}$  with 40 bunches, or  $\sim 2\%$  of the day-one target value. Since then, the luminosity has been raised slowly by abandoning attempts to provide simultaneous collisions at both IRs, adding octupole

magnets, correcting the poor wiggler field shape, improving injection efficiency, and installing a redesigned low- $\beta$  insertion at the KLOE IR. Even the KLOE field setting has been adjusted to optimize the luminosity (9). The integrated luminosity is maximized by frequently topping up the stored beams, without interrupting KLOE data taking. In 2000, an integrated luminosity of  $24 \text{ pb}^{-1}$  was delivered. This data set was used to obtain the first generation of KLOE results.

DAΦNE performance improved considerably year by year from 2001 to 2005. Figure 2 illustrates the growth of the KLOE data set.

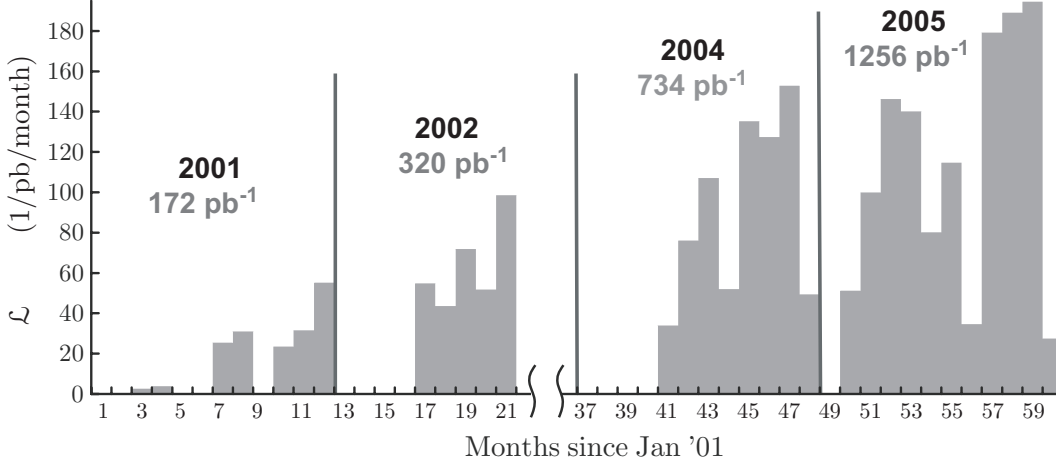


**Fig. 2.** Luminosity integrated by KLOE from 2001 to 2005.

In 2002,  $107 \text{ pb}^{-1}$  were delivered to DEAR. The first physics run with FINUDA began in November 2003 and ended in March 2004; a total of  $250 \text{ pb}^{-1}$  were delivered. From May 2004 to December 2005, DAΦNE operations were dedicated to KLOE data taking. In a single month near the end of this period (November 2005), KLOE collected  $190 \text{ pb}^{-1}$ , with sustained luminosities regularly in excess of  $10^{32} \text{ cm}^{-2} \text{ s}^{-1}$  and a one-day integrated-luminosity record of  $8.8 \text{ pb}^{-1}$ . During the 2004–2005 run, KLOE collected  $1.99 \text{ fb}^{-1}$ .

### 3 THE KLOE EXPERIMENT

At DAΦNE,  $\phi$  mesons decay nearly at rest.<sup>1</sup> Neutral and charged kaons from  $\phi$  decays have momenta of 110 and 127 MeV, respectively. As a result, the mean  $K_L$ ,  $K_S$ , and  $K^\pm$  decay path lengths are  $\lambda_L = 3.4 \text{ m}$ ,  $\lambda_S = 0.59 \text{ cm}$ , and  $\lambda_\pm = 95 \text{ cm}$ . A detector with a radius of  $\sim 2 \text{ m}$  is required to define a fiducial volume for the detection of  $K_L$  decays with a geometrical efficiency of  $\sim 30\%$ . Because the radial distribution of the  $K_L$  decay points is essentially uniform within this volume, tracks must be well reconstructed independently of their angles of emission, and photon vertices must be localized. To observe  $K_S$  decays and  $K_S K_L$  interference patterns with minimal complications from  $K_L \rightarrow K_S$  regeneration, a decay volume about the interaction point with  $r \gtrsim 10\lambda_S$  must remain in vacuum. Material within the sensitive volume must be kept to a minimum to reduce the effects of regeneration, photon conversion, and multiple scattering and energy loss for low-momentum charged particles.

<sup>1</sup>Because of the beam-crossing angle,  $\phi$ s have a net momentum of 12–16 MeV in the horizontal plane and directed towards the center of the rings. This momentum is determined run by run from Bhabha scattering events with a precision of 0.01 MeV.

Figure 3 shows a diagram of the cross section of the KLOE detector. The detector consists principally of a large drift chamber (DC) surrounded by a hermetic electromagnetic calorimeter (EMC). A superconducting coil surrounding the calorimeter provides an axial magnetic field of 0.52 T.

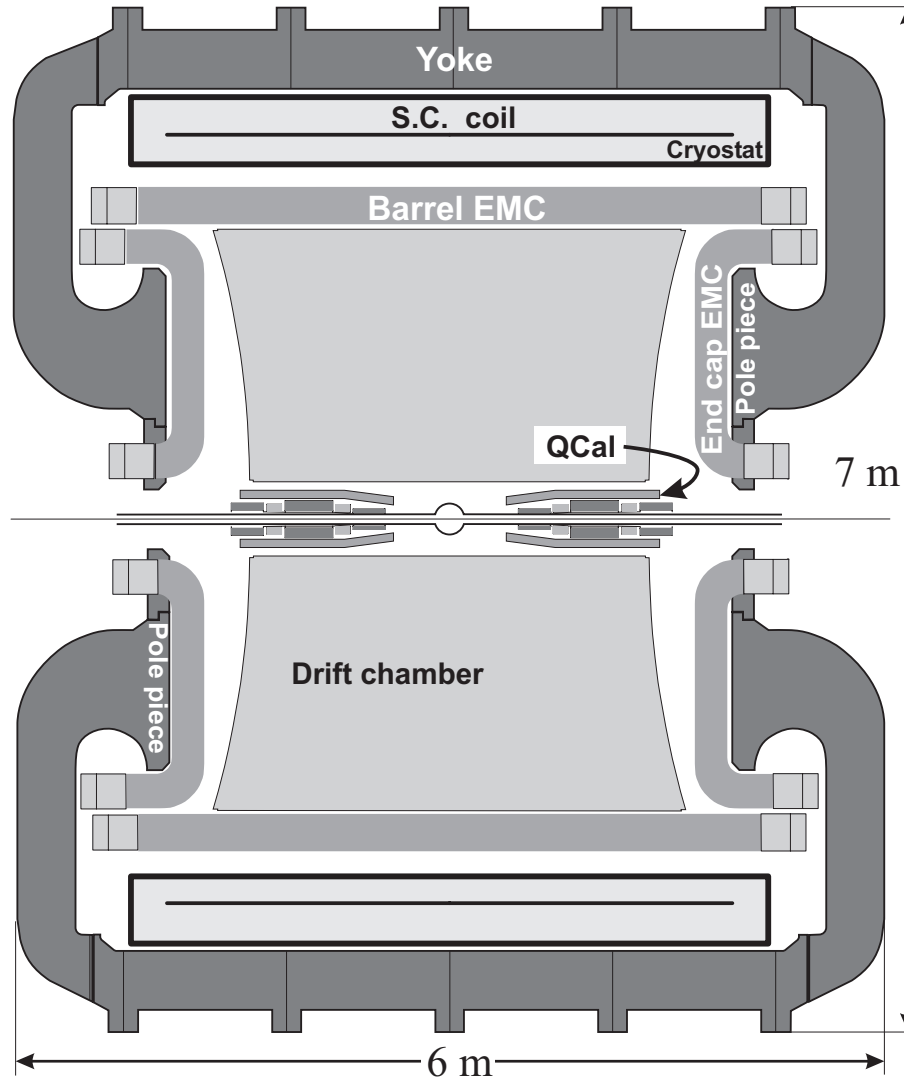


**Fig. 3.** Cross-sectional view of the KLOE experiment, showing the interaction region, the drift chamber (DC), the electromagnetic calorimeter (EMC), the superconducting coil, and the return yoke of the magnet.

The DC is 3.3 m long, with inner and outer radii of 25 and 200 cm, respectively. It contains 12,582 drift cells arranged in 58 stereo layers, for a total of 52,140 wires. The absolute value of the stereo angle increases from 60 to 150 mrad with the layer radius, and the sign of the stereo angle alternates from layer to layer. The difference between the radial distance from the chamber axis to the wires on a given layer as measured at the endplates and at the midpoint of the chamber is the same for all layers (1.5 cm). This design results in uniform filling of the sensitive volume, which increases the isotropy of the tracking efficiency. The cells are approximately square in shape; those in the first 12

layers measure  $2 \times 2 \text{ cm}^2$  in cross section, whereas those in the remaining 46 layers measure  $3 \times 3 \text{ cm}^2$ . The chamber uses a gas mixture of 90% helium and 10% isobutane. This reduces regeneration and multiple scattering within the chamber, while providing good spatial resolution ( $150 \text{ } \mu\text{m}$ ). Large-angle tracks from the origin ( $\theta > 45^\circ$ ) are reconstructed with  $\sigma_p/p < 0.4\%$ , and vertices within the sensitive volume are reconstructed with a position resolution of  $\sim 3 \text{ mm}$ . Groups of 12 consecutive wires on each layer are read out by analog-to-digital-converter electronics; the measurement of the specific ionization allows identification of  $K^\pm$  tracks by  $dE/dx$  alone. A full description of the design and operation of the chamber can be found in Reference 10.

The calorimeter is made of cladbed, 1-mm scintillating fibers sandwiched between 0.5-mm-thick lead foils. The foils are imprinted with grooves wide enough to accommodate the fibers and some epoxy, without compressing the fibers. This precaution prevents damage to the fiber-cladding interface. The epoxy around the fibers also provides structural strength and removes light traveling in the cladding. Many such layers are stacked, glued, and pressed, resulting in a bulk material with a radiation length  $X_0$  of 1.5 cm and an electromagnetic sampling fraction of  $\sim 13\%$ . This material is fashioned into modules 23 cm thick ( $\sim 15X_0$ ), 24 of which are arranged in azimuth to form the calorimeter barrel, and an additional 32 of which are wrapped around each of the pole pieces of the magnet yoke to form the endcaps. The unobstructed solid-angle coverage of the calorimeter as viewed from the origin is  $\sim 94\%$ . The fibers run parallel to the axis of the detector in the barrel, run vertical in the endcaps, and are read out at both ends with a granularity of  $4.4 \times 4.4 \text{ cm}^2$  by a total of 4880 photomultiplier tubes. Cluster energies are measured with a resolution of  $\sigma_E/E = 5.7\%/\sqrt{E \text{ (GeV)}}$ , as determined with the help of the DC using radiative Bhabha events. The absolute time resolution is  $\sigma_t = 54 \text{ ps}/\sqrt{E \text{ (GeV)}} \oplus 140 \text{ ps}$ , as determined from radiative  $\phi$  decays. The constant term results largely from the uncertainty of the event  $t_0$  arising from the length of the DAΦNE bunches. The constant contribution to the relative time resolution as determined using  $2\gamma$  events is  $\sim 50 \text{ ps}$ . Cluster positions are measured with resolutions of 1.3 cm in the coordinate transverse to the fibers, and, by timing, of  $1.2 \text{ cm}/\sqrt{E \text{ (GeV)}}$  in the longitudinal coordinate. These characteristics enable the  $2\gamma$  vertex in  $K_L \rightarrow \pi^+\pi^-\pi^0$  decays to be localized with  $\sigma \approx 2 \text{ cm}$  along the  $K_L$  line of flight, as reconstructed from the tagging  $K_S$  decay. The calorimeter is more fully described in Reference 11.

Around the interaction point, the beam pipe is spherical in shape, with a radius of 10 cm, so that all  $K_S$  mesons decay in vacuum. The beam-pipe walls are made of a 60%-beryllium/40%-aluminum alloy 0.5 mm thick. The quadrupoles of the low- $\beta$  insertion are covered with a lead/scintillating-tile calorimeter (12) intended to detect photons that are otherwise absorbed on the quadrupoles.

The two-level KLOE trigger (13) uses information from both the calorimeter and the DC. The level-1 trigger provides a fast response to initiate conversion in the front-end electronics modules. It is satisfied by two energy deposits above a threshold of 50 MeV on the EMC barrel and above 150 MeV on the endcaps, or by  $\sim 15$  hits in the DC arriving within a time window of 250 ns. All detector signals are digitized by KLOE-designed modules that can operate on signals arriving before the level-1 trigger. The level-2 trigger initiates event read out. In a typical configuration, the level-1 EMC signal satisfies level 2, whereas for the DC,  $\sim 120$  hits must arrive within a  $1.2\text{-}\mu\text{s}$  window. The trigger also implements logic to identify cosmic-ray events, which are recognized by the presence of two energy deposits above 30 MeV in the outermost calorimeter plane.

At a luminosity of  $10^{32} \text{ cm}^{-2} \text{ s}^{-1}$ , events are recorded at  $\sim 2200 \text{ Hz}$ . Of this rate,  $\sim 300 \text{ Hz}$  are from  $\phi$  decays. Raw data, reconstructed data, and Monte Carlo (MC) events occupy

$\sim 800$  TB and are stored in a tape library. Data summary tapes for both data and MC occupy  $\sim 80$  TB and are cached on disk for analysis. For a detailed description of the data acquisition, online, and offline systems, see References 14 and 15.

## 4 KAON PHYSICS

### 4.1 Why a $\phi$ Factory?

Interest in a  $\phi$  factory (16,17,18) is due to the fact that  $\phi$  mesons are produced abundantly in  $e^+e^-$  collisions. The visible cross section for  $e^+e^- \rightarrow \phi$  peaks at  $\sim 3 \mu\text{b}$  at  $\sqrt{s} \approx 1019.4$  MeV. For comparison,  $\sigma(e^+e^- \rightarrow \text{hadrons}) \approx 0.1 \mu\text{b}$ , and  $\sigma(e^+e^- \rightarrow e^+e^-, \theta > 20^\circ) \approx 7 \mu\text{b}$ . The  $\phi$  meson decays dominantly to charged kaon pairs (49%), neutral kaon pairs (34%),  $\rho\pi$  (15%), and  $\eta\gamma$  (1.3%). A  $\phi$  factory is thus a copious source of tagged and monochromatic kaons, both neutral and charged, and even a source of  $\eta$  mesons.

**4.1.1 TAGGED KAON BEAMS** Because the neutral kaon pair from  $\phi \rightarrow K^0 \bar{K}^0$  is purely  $J^{PC}=1^{--}$ , the initial two-kaon state can be written as

$$|K\bar{K}, t=0\rangle = (|K^0 \bar{K}^0\rangle - |\bar{K}^0 K^0\rangle)/\sqrt{2} \equiv (|K_S K_L\rangle - |K_L K_S\rangle)/\sqrt{2}, \quad (1)$$

where the identity holds even without assuming  $CPT$  invariance. Detection of a  $K_S$  ( $K_L$ ) thus signals the presence of a  $K_L$  ( $K_S$ ). This in effect creates pure  $K_S$  and  $K_L$  beams of precisely known momenta (event by event, from kinematic closure) and flux, which can be used to measure absolute  $K_S$  and  $K_L$  BRs, or, with even greater precision, ratios of such BRs. Similar arguments hold for  $K^+$  and  $K^-$  as well.

**4.1.2  $K_S K_L$  INTERFEROMETRY** Assuming  $CPT$  invariance, to lowest order in  $\epsilon$ , the states  $|K_S\rangle$  and  $|K_L\rangle$  are given by (16,18)

$$|K_S\rangle = \frac{(1+\epsilon)|K^0\rangle + (1-\epsilon)|\bar{K}^0\rangle}{\sqrt{N}}, \quad |K_L\rangle = \frac{(1+\epsilon)|K^0\rangle - (1-\epsilon)|\bar{K}^0\rangle}{\sqrt{N}}, \quad (2)$$

where  $N = 2(1+|\epsilon|^2)$ . If  $CPT$  invariance is not assumed, then ( $N$  changes):

$$|K_S\rangle = \frac{(1+\epsilon_S)|K^0\rangle + (1-\epsilon_S)|\bar{K}^0\rangle}{\sqrt{N}}, \quad |K_L\rangle = \frac{(1+\epsilon_L)|K^0\rangle - (1-\epsilon_L)|\bar{K}^0\rangle}{\sqrt{N}}. \quad (3)$$

It is normal to define the parameters  $\tilde{\epsilon}$  and  $\delta$  through the identities

$$\epsilon_S \equiv \tilde{\epsilon} + \delta; \quad \epsilon_L \equiv \tilde{\epsilon} - \delta. \quad (4)$$

We evolve the initial state in Equation 1 in time, project to any two possible final states  $f_1$  and  $f_2$ , take the modulus squared, and integrate over all  $t_1$  and  $t_2$  for fixed  $\Delta t = t_1 - t_2$  to obtain (for  $\Delta t > 0$ , with  $\Gamma \equiv \Gamma_L + \Gamma_S$ )

$$I_{f_1, f_2}(\Delta t) = \frac{1}{2\Gamma} |\langle f_1 | K_S \rangle \langle f_2 | K_S \rangle|^2 \times \left[ |\eta_1|^2 e^{-\Gamma_L \Delta t} + |\eta_2|^2 e^{-\Gamma_S \Delta t} - 2|\eta_1||\eta_2| e^{-(\Gamma_L + \Gamma_S)\Delta t/2} \cos(\Delta m \Delta t + \phi_2 - \phi_1) \right]. \quad (5)$$

The last term is due to interference between the decays to states  $f_1$  and  $f_2$ . Fits to the  $\Delta t$  distribution provide measurements of the magnitudes and phases of the parameters  $\eta_i = \langle f_i | K_L \rangle / \langle f_i | K_S \rangle$ , as well as of the  $K_L$ - $K_S$  mass difference  $\Delta m$  and the decay rates  $\Gamma_L$  and  $\Gamma_S$ . Many examples are discussed in References 16, 19, and 21.



Such fits also allow tests of fundamental properties of quantum mechanics. For example, the persistence of quantum-mechanical coherence can be tested by choosing  $f_1 = f_2$ . In this case, because of the antisymmetry of the initial state and the symmetry of the final state, there should be no events with  $\Delta t = 0$ . Using the 2001–2002 data, KLOE has conducted a preliminary analysis of the  $\Delta t$  distribution for  $K_S K_L \rightarrow \pi^+ \pi^- \pi^+ \pi^-$  events that establishes the feasibility of such tests (23). The  $\Delta t$  distribution is fit with a function of the form of Equation 5, including the experimental resolution and a peak from  $K_L \rightarrow K_S$  regeneration in the beam pipe. The results are shown in Figure 4.

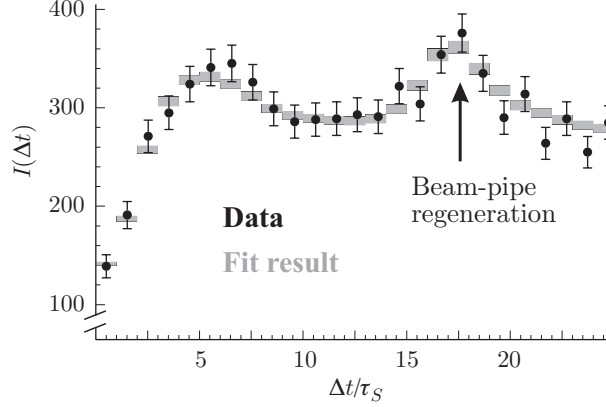


**Fig. 4.**  $\Delta t$  distribution for  $\phi \rightarrow K_S K_L \rightarrow \pi^+ \pi^- \pi^+ \pi^-$  events in  $380 \text{ pb}^{-1}$  of KLOE data.

**4.1.3 DIRECT  $CP$  VIOLATION IN NEUTRAL KAON DECAYS** Equation 2 gives the expressions for the mass eigenstates  $|K_S\rangle$  and  $|K_L\rangle$  assuming  $CPT$  invariance. If  $CP$  violation in the  $K_S K_L$  system results exclusively from mixing,  $\eta_{\pi^+ \pi^-} \equiv \eta_{+-} = \eta_{\pi^0 \pi^0} \equiv \eta_{00} = \epsilon$ . If  $CP$  is violated in the  $|\Delta S| = 1$  decay amplitudes, the amplitude ratios  $\eta$  are no longer equal and the magnitude of direct  $CP$  violation can be parameterized by  $\epsilon'$ :

$$\eta_{+-} = \epsilon + \epsilon'; \quad \eta_{00} = \epsilon - 2\epsilon'.$$

In the Standard Model, both  $\epsilon$  and  $\epsilon'$  are calculable in terms of the Cabibbo-Kobayashi-Maskawa (CKM) matrix elements. In general, if  $\epsilon$  is due to  $CP$  violation in the CKM matrix,  $\epsilon' \neq 0$ , except for fortuitous cancellations. There are no reliable calculations of  $\epsilon'$ . Experimentally,  $\text{Re } \epsilon'/\epsilon$  is obtained from the double ratio:

$$\mathcal{R} \equiv \frac{\Gamma(K_L \rightarrow \pi^0 \pi^0)/\Gamma(K_S \rightarrow \pi^0 \pi^0)}{\Gamma(K_L \rightarrow \pi^+ \pi^-)/\Gamma(K_S \rightarrow \pi^+ \pi^-)} \equiv \left| \frac{\eta_{00}}{\eta_{+-}} \right|^2 = 1 - 6 \text{Re } \epsilon'/\epsilon. \quad (6)$$

Recent results for  $\text{Re } \epsilon'/\epsilon$  from NA48 at CERN (24) and KTeV at Fermilab (25) are  $(14.7 \pm 2.2) \times 10^{-4}$  and  $(20.7 \pm 2.8) \times 10^{-4}$ , respectively. The two results are not in perfect agreement, but prove beyond any doubt the existence of direct  $CP$  violation; the observed value of  $\text{Re } \epsilon'/\epsilon$  is compatible with general expectations. The existence of direct  $CP$  violation cannot be confirmed at DAΦNE because of lack of luminosity. With sufficient data,  $\text{Re } \epsilon'/\epsilon$  would be measurable by Equation 6, and both  $\text{Re } \epsilon'/\epsilon$  and  $\text{Im } \epsilon'/\epsilon$  would be measurable by interferometry.

**4.1.4 KAON DECAYS AND DETERMINATION OF  $|V_{us}|$**  In the Standard Model, the quark weak charged current is

$$J_\alpha^+ = (\bar{u} \ \bar{c} \ \bar{t}) \gamma_\alpha (1 - \gamma_5) \mathbf{V} \begin{pmatrix} d \\ s \\ b \end{pmatrix},$$



where  $\mathbf{V}$  is a  $3 \times 3$  unitary matrix introduced by Kobayashi and Maskawa (26) in expansion on an original suggestion by Cabibbo (27). The unitarity condition ( $\mathbf{V}^\dagger \mathbf{V} = 1$ ) is required by the assumption of universality of the weak interactions of leptons and quarks and the absence of flavor-changing neutral currents. The realization that a precise test of CKM unitarity can be obtained from the first-row constraint  $|V_{ud}|^2 + |V_{us}|^2 + |V_{ub}|^2 = 1$  (with  $|V_{ub}|^2$  negligible) has sparked a new interest in good measurements of quantities related to  $|V_{us}|$ . As we discuss in the following sections,  $|V_{us}|$  can be determined using semileptonic kaon decays; the experimental inputs are the BRs, lifetimes, and form-factor slopes. Both neutral ( $K_S$  or  $K_L$ ) and charged kaons may be used and provide independent measurements. Many players have joined the game, as seen from Table 1.

Table 1. Recent world data on  $K_{\ell 3}$  decays for calculation of  $|V_{us}|$ 

Experiment	Parameters measured	References
E865	$\text{BR}(K^+ \rightarrow \pi_D^0 e^+ \nu) / \text{BR}(K^+ \rightarrow \pi_D^0 X^+)$	(28)
KTeV	$\text{BR}(K_{Le3}), \text{BR}(K_{L\mu 3}), \lambda_+(K_{Le3}), \lambda_{+,0}(K_{L\mu 3})$	(29,30)
ISTRA+	$\lambda_+(K_{e3}^-), \lambda_{+,0}(K_{\mu 3}^-)$	(31,32)
NA48	$\text{BR}(K_{Le3}) / \text{BR}(2 \text{ tracks}), \text{BR}(K_{e3}^\pm) / \text{BR}(\pi\pi^0), \lambda_+(K_{Le3})$	(33,35,36)
KLOE	$\text{BR}(K_{Le3}), \text{BR}(K_{L\mu 3}), \text{BR}(K_{Se3}), \text{BR}(K_{e3}^\pm), \text{BR}(K_{\mu 3}^\pm), \lambda_+(K_{Le3}), \tau_L, \tau^\pm$	See text

KLOE is unique in that it is the only experiment that can by itself measure the complete set of experimental inputs for the calculation of  $|V_{us}|$  using both charged and neutral kaons. This is because the  $\phi$  factory is uniquely suited for measurements of the  $K_L$  and  $K^\pm$  lifetimes. In addition, KLOE is the only experiment that can measure  $K_S$  BRs at the sub-percent level. We illustrate in Section 4.5 by calculating  $|V_{us}|$  from the comprehensive KLOE data set on semileptonic kaon decays.

One problem that consistently plagues the interpretation of older BR measurements is lack of clarity in the treatment of radiative contributions. All KLOE measurements of kaon decays with charged particles in the final state are fully inclusive of radiation. The inclusion of radiation is handled as an acceptance correction—the relevant MC generators incorporate radiation as described in Reference 37.

**4.1.5 SEMILEPTONIC KAON DECAYS** The semileptonic kaon decay rates still provide the best means for the measurement of  $|V_{us}|$  because only the vector part of the weak current contributes to the matrix element  $\langle \pi | J_\alpha | K \rangle$ . In general,

$$\langle \pi | J_\alpha | K \rangle = f_+(t)(P + p)_\alpha + f_-(t)(P - p)_\alpha,$$

where  $P$  and  $p$  are the kaon and pion four-momenta, respectively, and  $t = (P - p)^2$ . The form factors  $f_+$  and  $f_-$  appear because pions and kaons are not point-like particles, and also reflect both  $SU(2)$  and  $SU(3)$  breaking. For vector transitions, the Ademollo-Gatto theorem (38) ensures that  $SU(3)$  breaking appears only to second order in  $m_s - m_{u,d}$ . In particular,  $f_+(0)$  differs from unity by only 2–4%. When the squared matrix element is evaluated, a factor of  $m_\ell^2/m_K^2$  multiplies all terms containing  $f_-(t)$ . This form factor can be neglected for  $K_{e3}$  decays. For the description of  $K_{\mu 3}$  decays, it is customary to use  $f_+(t)$  and the scalar form factor  $f_0(t) \equiv f_+(t) + [t/(m_K^2 - m_\pi^2)] f_-(t)$ .

The semileptonic decay rates, fully inclusive of radiation, are given by

$$\Gamma^i(K_{e3}, \mu 3) = |V_{us}|^2 \frac{C_i^2 G^2 M^5}{768\pi^3} S_{\text{EW}} (1 + \delta_{i,\text{em}} + \delta_{i,SU(2)}) |f_+^{K^0}(0)|^2 I_{e3, \mu 3}. \quad (7)$$

In the above expression,  $i$  indexes  $K^0 \rightarrow \pi^\pm$  and  $K^\pm \rightarrow \pi^0$  transitions, for which  $C_i^2 = 1$  and  $1/2$ , respectively.  $G$  is the Fermi constant,  $M$  is the appropriate kaon mass, and  $S_{\text{EW}}$  is the universal short-distance radiative correction factor (39). The  $\delta$  terms are the long-distance radiative corrections, which depend on the meson charges and lepton masses, and the  $SU(2)$ -breaking corrections, which depend on the kaon charge (40). The form factors are written as  $f_{+,0}(t) = f_+(0)\tilde{f}_{+,0}(t)$ , with  $\tilde{f}_{+,0}(0) = 1$ .  $f_+(0)$  reflects  $SU(2)$ - and  $SU(3)$ -breaking corrections and is different for  $K^0$  and  $K^\pm$ .  $I_{e3,\mu3}$  is the integral of the Dalitz-plot density over the physical region and includes  $|\tilde{f}_{+,0}(t)|^2$ .  $I_{e3,\mu3}$  does not account for photon emission; the effects of radiation are included in the electromagnetic (em) corrections. The numerical factor in the denominator of Equation 7,  $768 = 3 \times 2^8$ , is chosen in such a way that  $I = 1$  when the masses of all final-state particles vanish. For  $K_{e3}$ ,  $I \approx 0.56$  and for  $K_{\mu3}$ ,  $I \approx 0.36$ . The vector form factor  $f_+$  is dominated by the vector  $K\pi$  resonances, the closest being the  $K^*(892)$ . Note that for  $t > 0$ ,  $\tilde{f}_+(t) > 1$ . The presence of the form factor increases the value of the phase-space integral and the decay rate. The natural form for  $\tilde{f}_+(t)$  is

$$\tilde{f}_+(t) = \frac{M_V^2}{M_V^2 - t}. \quad (8)$$

It is also customary to expand the form factor in powers of  $t$  as

$$\tilde{f}_+(t) = 1 + \lambda' \frac{t}{m_{\pi^+}^2} + \frac{\lambda''}{2} \left( \frac{t}{m_{\pi^+}^2} \right)^2.$$

To compare the results obtained from each semileptonic decay mode for both neutral and charged kaons without knowledge of  $f_+(0)$ , Equation 7 is usually used to compute the quantity  $f_+^{K^0}(0)|V_{us}|$ . This requires the  $SU(2)$  and electromagnetic corrections for all four possible cases.

**4.1.6  $K \rightarrow \mu\nu$  DECAYS** High-precision lattice quantum chromodynamics (QCD) results have recently become available and are rapidly improving (41). The availability of precise values for the pion- and kaon-decay constants  $f_\pi$  and  $f_K$  allows use of a relation between  $\Gamma(K_{\mu2})/\Gamma(\pi_{\mu2})$  and  $|V_{us}|^2/|V_{ud}|^2$ , with the advantage that lattice-scale uncertainties and radiative corrections largely cancel out in the ratio (42):

$$\frac{\Gamma(K_{\mu2}(\gamma))}{\Gamma(\pi_{\mu2}(\gamma))} = \frac{|V_{us}|^2}{|V_{ud}|^2} \frac{f_K^2}{f_\pi^2} \frac{m_K (1 - m_\mu^2/m_K^2)^2}{m_\pi (1 - m_\mu^2/m_\pi^2)^2} \times (0.9930 \pm 0.0035), \quad (9)$$

where the precision of the numerical factor due to structure-dependent corrections (43) can be improved. Thus, it could very well be that the abundant decays of pions and kaons to  $\mu\nu$  ultimately give the most accurate determination of the ratio of  $|V_{us}|$  to  $|V_{ud}|$ . This ratio can be combined with direct measurements of  $|V_{ud}|$  to obtain  $|V_{us}|$  using unitarity (42, 45). What is more interesting, however, is to combine all information from  $K_{e2}$ ,  $K_{\mu2}$ ,  $K_{e3}$ ,  $K_{\mu3}$ , and superallowed  $0^+ \rightarrow 0^+$  nuclear  $\beta$ -decays to experimentally test electron-muon and lepton-quark universality, in addition to the unitarity of the quark mixing matrix.

## 4.2 $K_L$ Decays

**4.2.1 MEASUREMENTS OF  $K_L$  PROPERTIES** Not all parameters describing the  $K_S K_L$  system are measurable from the study of  $\phi \rightarrow K_S K_L$  decays without assuming either  $CPT$  invariance or the  $\Delta S = \Delta Q$  rule. The set can be made complete at DAΦNE by

including measurements of the  $\Delta S \neq \Delta Q$  amplitude using strangeness-tagged  $K^0$  and  $\bar{K}^0$  mesons from charge exchange of tagged  $K^\pm$  mesons. We are mostly interested here in the quantities relevant to the measurement of  $|V_{us}|$ . For  $K_L$  mesons, the necessary quantities are the neutral kaon mass, the  $K_L$  lifetime, the semileptonic BRs, and the slopes of the hadronic-current form factors. KLOE finds  $m_{K_L} = 497.583 \pm 0.021$  MeV (46, 47). This value is accurately determined owing to the precise Novosibirsk measurement of the  $\phi$  mass (48) and the smallness of  $m_\phi - 2m_{K^0} = 24.317$  MeV. Knowledge of the mass is necessary for the phase-space integrals, for the BR measurements, for the correct evaluation of the  $M^5$  factor in Equation 7, and for the evaluation of the radiative corrections.

**4.2.2  $K_L$  LIFETIME** The  $K_L$  lifetime is particularly difficult to measure because monochromatic neutral kaons are generally not available, nor can they be stopped. In addition, only a small fraction of the  $K_L$  lifetime is covered in a typical experiment. If  $N$  events are observed in a time window of  $T$  lifetimes (with  $T \ll 1$ ), and the lifetime is determined from a fit to the proper-time distribution, the fractional error is  $\delta\tau/\tau = 2\sqrt{3}/(T\sqrt{N})$ . A good measurement is possible at DAΦNE, where a monochromatic beam of very slow  $K_L$ s is available. KLOE can cover  $\sim 37\%$  of the  $K_L$  lifetime, compared with a few percent in KTeV or NA48. KLOE has performed a fit to the proper-time distribution for  $K_L \rightarrow 3\pi^0$  decays, which can be isolated with high purity and high and uniform efficiency (49). The fit to the distribution for  $\sim 10$  million  $K_L \rightarrow 3\pi^0$  decays ( $400 \text{ pb}^{-1}$ ) in the proper-time interval from 6 to 25 ns gives  $\tau_{K_L} = 50.92 \pm 0.30$  ns. The fractional statistical error is  $\sim 10.5/\sqrt{N} \approx 0.33\%$ . The stated error on  $\tau_{K_L}$  includes a systematic uncertainty of 0.5%.

If, as at a  $\phi$  factory, the total number of  $K_L$ s created is known, the lifetime can also be obtained from the number of decays  $N_D$  in a time interval  $\Delta$  beginning at time  $t$ . The fractional error is given by

$$\frac{\delta\tau}{\tau} = \frac{\delta\Gamma}{\Gamma} \approx \frac{1}{\sqrt{N_D}} \left| \frac{1 - e^{-\Gamma\Delta}}{(\Gamma t + \Gamma\Delta)e^{-\Gamma\Delta} - \Gamma t} \right|.$$

For KLOE,  $\Gamma t \approx 0.12$  and  $\Gamma\Delta \approx 0.37$ , so  $\delta\tau/\tau \approx 1.4/\sqrt{N_D}$ . Using this method, KLOE finds  $\tau_{K_L} = 50.72 \pm 0.36$  ns (see Section 4.2.3). Because the two determinations are almost entirely uncorrelated and the errors are dominated by different systematic uncertainties, the two values can be averaged. KLOE obtains  $\tau_{K_L} = 50.84 \pm 0.23$ , which is a factor of  $\sim 2$  improvement over the 1972 measurement of Vosburgh et al. (50).

**4.2.3  $K_L$  BRANCHING RATIOS** The KLOE measurements of the semileptonic  $K_L$  BRs (51) are based on two points. The first, unique to DAΦNE and KLOE, is the use of tagging to obtain absolute BRs; the presence of a  $K_L$  is tagged by observation of a  $K_S \rightarrow \pi^+\pi^-$  decay. The second point is that just four modes,  $\pi^\pm e^\mp \nu$  ( $K_{e3}$ ),  $\pi^\pm \mu^\mp \nu$  ( $K_{\mu3}$ ),  $\pi^+\pi^-\pi^0$ , and  $3\pi^0$ , account for more than 99.5% of all decays. For the first three modes, two tracks are observed in the DC, whereas for the  $3\pi^0$  mode, only photons appear in the final state. The analysis of two-track and all-neutral-particle events is quite different. The main experimental problem is ensuring that the tagging is bias free. Because both the trigger and reconstruction efficiencies for  $K_S \rightarrow \pi^+\pi^-$  decays exhibit some dependence on the  $K_L$  decay mode to be identified, most of the analysis revolves around minimizing and correcting the tag bias.

To deal properly with this problem, two more possibilities for the behavior of the  $K_L$  must be included: The  $K_L$  may reach the calorimeter and interact, or it may escape the detector altogether. We define the tag bias  $B_i$  for  $K_L$  channel  $i$  as one minus the ratio of the  $K_S$  detection efficiency when  $K_L \rightarrow i$  to the  $K_S$  detection efficiency averaged over all possible  $K_L$  “channels,” including the last two listed above. The tag bias is minimized by retaining only events in which it is possible to verify that the  $K_S \rightarrow \pi^+\pi^-$  decay satisfied

the calorimeter trigger by itself. MC simulations give  $B_i \approx 0.03$  for the two-track  $K_L$  decays, and  $B_i \approx 0.00$  for  $3\pi^0$ . A correction of  $+0.2\%$  to the average tagging efficiency is obtained from data. An additional correction of approximately  $-0.5\%$ , also obtained from data, accounts for decreased reconstruction efficiency for the tracks from  $K_S \rightarrow \pi^+\pi^-$ , owing to the presence of the  $K_L$  decay products. This last correction depends on the DAΦNE operating conditions and is obtained separately for different sets of runs.

Two-track events are assigned to the three channels of interest by use of a single variable: the smaller absolute value of the two possible values of  $\Delta_{\mu\pi} = |\mathbf{p}_{\text{miss}}| - E_{\text{miss}}$ , where  $\mathbf{p}_{\text{miss}}$  and  $E_{\text{miss}}$  are the missing momentum and energy in the  $K_L$  decay, respectively, and are evaluated assuming the decay particles are a pion and a muon. Figure 5 (left panel) shows an example of a  $\Delta_{\mu\pi}$  distribution. A total of approximately 13 million tagged  $K_L$  decays ( $328 \text{ pb}^{-1}$ ) are used for the measurement of the BRs. The numbers of  $K_{e3}$ ,  $K_{\mu 3}$ , and  $\pi^+\pi^-\pi^0$  decays are obtained separately for each of 14 run periods by fitting the  $\Delta_{\mu\pi}$  distribution with the corresponding MC-predicted shapes. The signal extraction procedure is tested using particle-identification variables from the calorimeter. Figure 5 (right panel) shows the  $\Delta_{e\pi}$  spectrum for events with identified electrons, together with the results of a fit using MC shapes. The  $K_{e3(\gamma)}$  radiative tail is clearly evident. The inclusion of radiative processes in the simulation is necessary to obtain an acceptable fit, as well as to properly estimate the fully inclusive radiative rates.

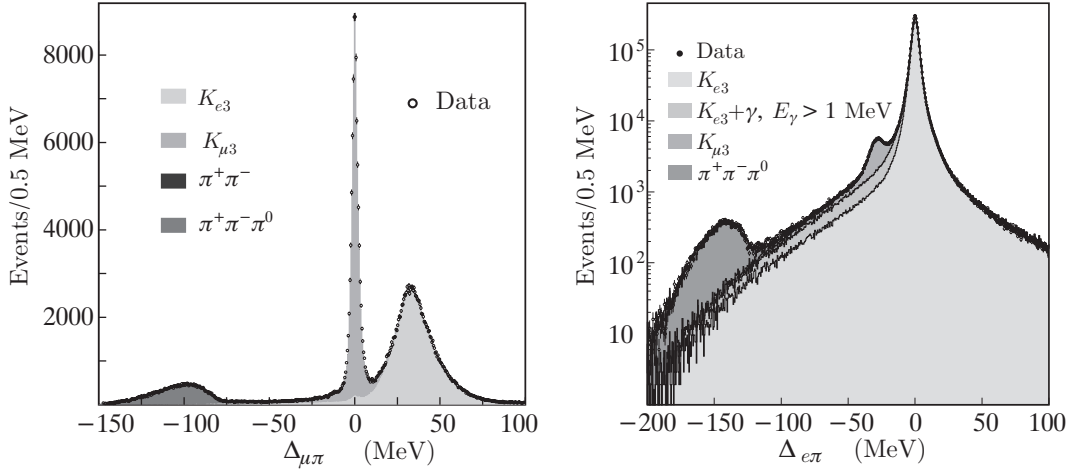


**Fig. 5.** (*Left panel*) Distribution of  $\Delta_{\mu\pi}$  for a run set. (*Right panel*) Distribution of  $\Delta_{e\pi}$  for events with an identified electron, for the entire data set.

The decay  $K_L \rightarrow 3\pi^0$  is easier to identify. Detection of  $\geq 3$  photons originating at the same point is accomplished with very high efficiency (99%) and very little background (1.1%). Changing the required number of photons from three to five reduces the background to 0.1%, with a detection efficiency of 88%. This variation in the selection criteria changes the result by 1%. This entire change is taken as the magnitude of the systematic uncertainty on the corresponding BR.

To conveniently estimate the individual efficiencies, the BRs are obtained using the  $K_L$  lifetime measurement of Vosburgh et al. (50):  $\tau_{K_L} = 51.54 \pm 0.44 \text{ ns}$ . The errors on the absolute BRs are dominated by the uncertainty on the value of  $\tau_{K_L}$ , which enters into the calculation of the geometrical efficiency. This source of uncertainty can be all but removed (at the cost of correlating the errors among the BR measurements) by applying the constraint that the  $K_L$  BRs must sum to unity. The sum of the four BRs, plus the

sum of the Particle Data Group (PDG) values (52) for  $K_L$  decays to  $\pi^+\pi^-$ ,  $\pi^0\pi^0$ , and  $\gamma\gamma$  ( $\Sigma=0.0036$ ), is  $1.0104 \pm 0.0018 \pm 0.0074$ .<sup>2</sup> Applying the constraint gives the results in Table 2.

 Table 2. KLOE measurements of  $K_L$  branching ratios

Mode	BR	$\delta$ stat	$\delta$ syst-stat	$\delta$ syst
$\pi^\pm e^\mp \nu$	0.4007	0.0005	0.0004	0.0014
$\pi^\pm \mu^\mp \nu$	0.2698	0.0005	0.0004	0.0014
$\pi^0 \pi^0 \pi^0$	0.1997	0.0003	0.0004	0.0019
$\pi^+ \pi^- \pi^0$	0.1263	0.0004	0.0003	0.0011

Constraining the BRs to sum to unity and solving for the geometrical efficiency is equivalent to determining  $\tau_{K_L}$  by the second method described in Section 4.2.2. KLOE finds  $\tau_{K_L} = 50.72 \pm 0.17 \pm 0.33$  ns.

For the ratio  $\Gamma(K_{\mu 3})/\Gamma(K_{e 3})$ , KLOE obtains  $R_{\mu e} = 0.6734 \pm 0.0059$ . A value for comparison can be computed from the slope of the  $f_0$  form factor. The average of the measurements of  $\lambda_0$  from the KTeV experiment at Fermilab (30) and the ISTRA+ experiment at Protvino (32) gives  $R_{\mu e} = 0.6640 \pm 0.0040$ . For the ratio  $\Gamma(K_L \rightarrow \pi^0 \pi^0 \pi^0)/\Gamma(K_L \rightarrow \pi^+ \pi^- \pi^0)$ , KLOE obtains  $R_{3\pi} = 1.582 \pm 0.027$ . A value for comparison,  $R_{3\pi} = 1.579$ , has been obtained from the isospin amplitudes derived from BRs and Dalitz-plot slopes for  $K \rightarrow 3\pi$  decays (53).

**4.2.4 THE VECTOR FORM FACTOR  $\tilde{f}_+(t)$  FOR  $K_{e 3}$  DECAYS** As discussed in Section 4.1.5, knowledge of the form factor is necessary to compute the phase-space integral that appears in Equation 7. This measurement is particularly delicate; it took more than 50 years to obtain reliable results. One reason is that in the expression for the pion energy spectrum, the form factor is multiplied by the kinematic density of the modulus-squared matrix element  $|\mathfrak{M}|^2$ . It so happens that the kinematic density vanishes for  $t = t_{\max}$ , precisely where the form factor itself is maximal. Therefore, the effect of the form factor on the shape of the pion spectrum is very small, as seen from Figure 6 (left panel). The right panel of Figure 6 compares KLOE results for  $\lambda'_+$  and  $\lambda''_+$  (54) with those from other experiments (30, 31, 32, 36).

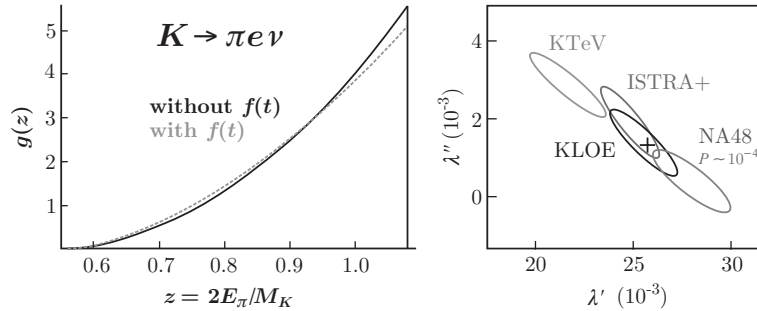


**Fig. 6.** (Left panel) Normalized pion spectra for  $K \rightarrow \pi e \nu$  decays, with  $\lambda'_+ = \lambda''_+ = 0$  and  $\lambda'_+ = 0.0221$ ,  $\lambda''_+ = 0.0023$ . (Right panel) KLOE  $1\sigma$  contours for  $\lambda'_+$  and  $\lambda''_+$ , compared with other results. The cross gives the KLOE values obtained for a pole fit.

<sup>2</sup>Throughout this article, whenever two errors are quoted on a measured quantity, the first error is statistical and the second is systematic, unless otherwise indicated.

The KLOE results for the slope and curvature parameters are  $\lambda'_+ = (25.5 \pm 1.5 \pm 1.0) \times 10^{-3}$  and  $\lambda''_+ = (1.4 \pm 0.7 \pm 0.4) \times 10^{-3}$ , respectively, with  $\chi^2/\text{ndf} = 325/362$  ( $P(\chi^2) = 91.9\%$ ). The data have also been fit using the one-pole parameterization (Equation 8). The result is  $M_V = 870 \pm 6 \pm 7$  MeV; the fit gives  $\chi^2/\text{ndf} = 326/363$  ( $P(\chi^2) = 92.4\%$ ).

### 4.3 $K_S$ Decays

The possibility of tagging a pure  $K_S$  beam is unique to a  $\phi$  factory. At KLOE, a particularly clean tag for  $K_S$  decays is obtained by observing the interaction of a  $K_L$  in the EMC, referred to as a “ $K_L$  crash.” The  $K_L$  crash is recognized as an isolated, high-energy (typically,  $E > 100$  MeV) cluster that arrives roughly 24 ns after the clusters from the  $K_S$  decay, as expected for a neutral particle with  $\beta \approx 0.2$ . The tagging efficiency is approximately 30% and is dominated by the probability for the  $K_L$  to reach the calorimeter. The position of the  $K_L$  crash, together with the kinematics of the  $\phi \rightarrow K_S K_L$  decay, determines the trajectory of the  $K_S$  with a momentum resolution of approximately 1 MeV and an angular resolution of better than  $1^\circ$ . The simulation of the EMC response to the  $K_L$  crash in the KLOE MC has been adjusted carefully with reference to data (55). KLOE has used the  $K_L$ -crash tag to obtain  $K_S$  BR measurements spanning six orders of magnitude.

**4.3.1  $K_S \rightarrow \pi^+\pi^-(\gamma)$ ,  $\pi^0\pi^0$**  The two channels  $\pi^+\pi^-$  and  $\pi^0\pi^0$  comprise  $\sim 99.9\%$  of all  $K_S$  decays. The rates for the  $K_S \rightarrow \pi\pi$  decays, together with the much slower rate for  $K^\pm \rightarrow \pi^\pm\pi^0$ , first suggested the empirical rule that  $\Delta I = 1/2$  transitions are much favored over  $\Delta I = 3/2$  transitions. This is true in all  $|\Delta S| = 1$  transitions; the phenomenon remains poorly understood.

The ratio  $R_\pi \equiv \Gamma(K_S \rightarrow \pi^+\pi^-(\gamma))/\Gamma(K_S \rightarrow \pi^0\pi^0)$  is a fundamental parameter of the  $K_S$  meson. With almost no corrections, its measurement provides the BRs for the dominant  $K_S$  decays to  $\pi^0\pi^0$  and  $\pi^+\pi^-(\gamma)$ . The latter decay is a convenient normalization reference for all other  $K_S$  decays to charged particles (see Section 4.3.2).  $R_\pi$  is also used in the extraction of values for phenomenological parameters of the kaon system, such as the differences in magnitude and phase of the  $I = 0, 2$   $\pi\pi$  scattering amplitudes (see, e.g., Reference 56). Finally,  $R_\pi$  enters in the double ratio of Equation 6, which measures direct  $CP$  violation in  $K \rightarrow \pi\pi$  transitions.

A first KLOE measurement of  $R_\pi$  based on  $17 \text{ pb}^{-1}$  of data from 2000, gave the result  $R_\pi = 2.236 \pm 0.003 \pm 0.015$  (57). This result increased the PDG average for  $R_\pi$  by 0.028, and correspondingly changed the PDG fit values for  $\text{BR}(K_S \rightarrow \pi^+\pi^-)$  and  $\text{BR}(K_S \rightarrow \pi^0\pi^0)$  by +0.5% and  $-1.1\%$ , respectively (52). The  $1.3\sigma$  difference between the KLOE value and older values is believed to arise from the imprecise treatment of the contribution from  $\pi^+\pi^-\gamma$  in the older measurements. KLOE has nonzero acceptance over the entire range of photon energies for  $K_S \rightarrow \pi^+\pi^-\gamma$  decays, and the KLOE measurement of  $R_\pi$  is fully inclusive. The analysis has recently been repeated using  $410 \text{ pb}^{-1}$  of 2001–2002 data (58). The value obtained for  $R_\pi$  is  $2.2555 \pm 0.0024 \pm 0.0050$ . Because the uncertainty on this result is dominated entirely by experimental systematics, the increase in statistics provided by the 2001–2002 data is used to obtain highly accurate corrections directly from the data itself. This, together with various improvements to the analysis, leads to the significant reduction in the systematic error. The new result is consistent with the previous KLOE value; the overall error has been reduced to 0.25%. Combining the two results with attention to the common systematic errors gives  $R_\pi = 2.2549 \pm 0.0054$ .

**4.3.2  $K_S \rightarrow \pi e \nu(\gamma)$**  Using the  $K_L$ -crash tag, KLOE has isolated a very pure sample of  $\sim 13,000$  semileptonic  $K_S$  decays and accurately measured the BRs for  $K_S \rightarrow \pi^+ e^- \bar{\nu}(\gamma)$



and  $K_S \rightarrow \pi^- e^+ \nu(\gamma)$ .

Discrete symmetries can be tested by comparing the charge asymmetries  $A_S$  and  $A_L$ , defined as the difference between the widths for  $K_S$  or  $K_L$  decays to final states of each lepton charge, divided by their sum.  $A_L$  is known to an absolute accuracy of  $\mathcal{O}(10^{-4})$  (59), whereas  $A_S$  has never previously been measured. If  $CPT$  invariance holds, the two charge asymmetries are equal to  $2 \operatorname{Re} \epsilon \approx 3 \times 10^{-3}$ . A difference between  $A_S$  and  $A_L$  signals  $CPT$  violation either in the mass matrix or in the  $\Delta S \neq \Delta Q$  decay amplitudes:

$$A_S - A_L = 4(\operatorname{Re} \delta + \operatorname{Re} x_-). \quad (10)$$

The parameter  $\delta$  is defined in Equations 2, 3, and 4.  $x_-$  is the ratio of the  $CPT$ -odd,  $\Delta S \neq \Delta Q$  decay amplitude to the  $CPT$ -even,  $\Delta S = \Delta Q$  decay amplitude. The most precise test of  $CPT$  invariance in  $K^0 \bar{K}^0$  mixing comes from the CPLEAR experiment at CERN (60). They find  $\operatorname{Re} \delta$  and  $\operatorname{Re} x_-$  consistent with zero, with sensitivities of  $3 \times 10^{-4}$  and  $10^{-2}$ . The sum of the asymmetries gives

$$A_S + A_L = 4(\operatorname{Re} \epsilon - \operatorname{Re} y), \quad (11)$$

where  $y$  is the ratio of  $CPT$ -odd to  $CPT$ -even  $\Delta S = \Delta Q$  decay amplitudes. The value of  $\operatorname{Re} y$  from unitarity (61) is zero to within  $3 \times 10^{-3}$ .

From the knowledge of the semileptonic partial widths for both the  $K_S$  and  $K_L$ , it is possible to test the validity of the  $\Delta S = \Delta Q$  rule under  $CPT$  invariance. With  $x_+$  as the ratio of the  $CPT$ -conserving amplitudes for  $\Delta S \neq \Delta Q$  and  $\Delta S = \Delta Q$  transitions,

$$\operatorname{Re} x_+ = \frac{1}{2} \frac{\Gamma(K_S \rightarrow \pi e \nu) - \Gamma(K_L \rightarrow \pi e \nu)}{\Gamma(K_S \rightarrow \pi e \nu) + \Gamma(K_L \rightarrow \pi e \nu)}. \quad (12)$$

In the Standard Model, a finite value of  $\operatorname{Re} x_+$  on the order of  $G_F m_\pi^2 \sim 10^{-7}$  arises from second-order weak processes. Previously, the most precise test of the  $\Delta S = \Delta Q$  rule was obtained from a study of strangeness-tagged semileptonic kaon decays by CPLEAR (62). CPLEAR finds  $\operatorname{Re} x_+$  compatible with zero to within  $6 \times 10^{-3}$ . The most precise previous measurement of  $\operatorname{BR}(K_S \rightarrow \pi e \nu)$  was obtained by KLOE using the data from 2000 ( $17 \text{ pb}^{-1}$ ) and had a fractional uncertainty of 5.4% (63). The 2001–2002 KLOE data set is  $\sim 20$  times larger, and the purity of the semileptonic decay sample has been vastly improved (64).

We outline briefly the basic steps in the analysis.  $K_S$  decays are tagged by the  $K_L$  crash. A cut on the  $\pi\pi$  invariant mass removes 95% of the  $K_S \rightarrow \pi^+ \pi^-$  decays and reduces the background-to-signal ratio to  $\sim 80:1$ . Several geometrical cuts further improve the purity of the sample and, in particular, remove contamination by events with early  $\pi \rightarrow \mu\nu$  decays. Finally, stringent requirements are imposed on the particle time of flight (TOF), which very effectively separates electrons from pions and muons and allows charge assignment of the final state. Figure 7 shows the signal peak and the residual background in the distribution of  $\Delta_{Ep} = E_{\text{miss}} - |\mathbf{p}_{\text{miss}}|$  for the  $\pi^- e^+ \nu$  channel, where  $E_{\text{miss}}$  and  $\mathbf{p}_{\text{miss}}$  are respectively the missing energy and momentum at the vertex, evaluated in the signal hypothesis. For signal events, the missing particle is a neutrino and  $\Delta_{Ep} = 0$ .



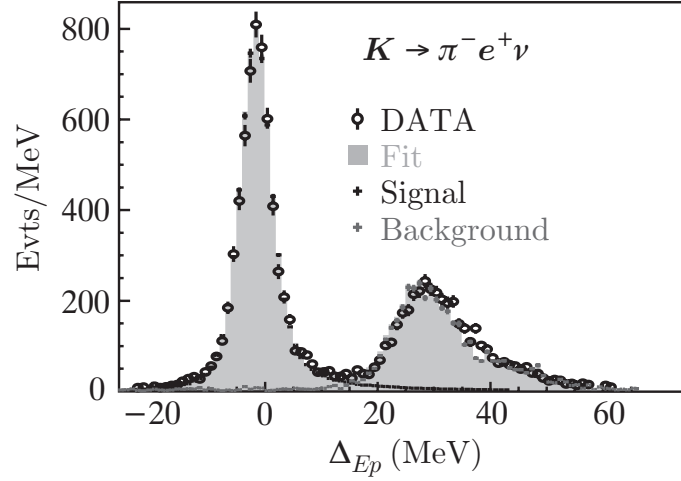


**Fig. 7.**  $\Delta_{Ep}$  distribution for  $K_S \rightarrow \pi^- e^+ \nu$  candidates, showing signal and background.

The numbers of  $\pi e \nu$  decays for each charge state are normalized to the number of  $\pi^+ \pi^-$  events observed, resulting in the ratios in the first column of Table 3. These ratios give the first measurement of the semileptonic charge asymmetry for the  $K_S$ :

$$A_S = (1.5 \pm 9.6 \pm 2.9) \times 10^{-3}.$$

Using the result for  $R_\pi$  of Section 4.3.1 (also in Table 3), the absolute BRs for  $K_S \rightarrow \pi \pi$  and  $K_S \rightarrow \pi e \nu$  in the second column of the table are obtained.

Table 3. KLOE measurements of  $K_S$  branching ratios

Decay mode	BR(mode)/BR( $\pi^+ \pi^-$ )	BR(mode)
$\pi^+ \pi^-$	—	$(69.196 \pm 0.024 \pm 0.045)\%$
$\pi^0 \pi^0$	$1/(2.2549 \pm 0.0054)$	$(30.687 \pm 0.024 \pm 0.045)\%$
$\pi^- e^+ \nu$	$5.099 \pm 0.082 \pm 0.039 \times 10^{-4}$	$3.528 \pm 0.057 \pm 0.027 \times 10^{-4}$
$\pi^+ e^- \bar{\nu}$	$5.083 \pm 0.073 \pm 0.042 \times 10^{-4}$	$3.517 \pm 0.050 \pm 0.029 \times 10^{-4}$
$\pi e \nu$	$10.19 \pm 0.11 \pm 0.07 \times 10^{-4}$	$7.046 \pm 0.076 \pm 0.051 \times 10^{-4}$

With  $\tau_{K_S}$  from the PDG (52) and  $\tau_{K_L}$  and  $\text{BR}(K_L \rightarrow \pi e \nu)$  from KLOE, Equation 12 gives  $\text{Re } x_+ = (-0.5 \pm 3.1 \pm 1.8) \times 10^{-3}$ , which is more precise than the CPLEAR value (62) by nearly a factor of two. Using Equation 10 to combine the KLOE result for  $A_S$  with the PDG value for  $A_L$  and with the CPLEAR value for  $\text{Re } \delta$  (60) gives  $\text{Re } x_- = (-0.8 \pm 2.4 \pm 0.7) \times 10^{-3}$ ; the uncertainty on this quantity is reduced by a factor of 10.  $A_S$  and  $A_L$ , together with the PDG value for  $\text{Re } \epsilon$  obtained without assuming  $CPT$  invariance ( $|\epsilon| \cos \phi_\epsilon = (1.62 \pm 0.04) \times 10^{-3}$ ), give  $\text{Re } y = (0.4 \pm 2.4 \pm 0.7) \times 10^{-3}$  (Equation 11), which is comparable in precision to the value obtained by CPLEAR using the unitarity relation (61).

**4.3.3  $K_S \rightarrow 3\pi^0$**  The decay  $K_S \rightarrow 3\pi^0$  is purely  $CP$  violating. If  $CPT$  is conserved, the BR for this decay can be predicted from  $\Gamma_S = \Gamma_L |\epsilon + \epsilon'_{000}|^2$ , giving  $\text{BR} \approx 1.9 \times 10^{-9}$ . In KLOE, the signature is an event with a  $K_L$  crash, six photon clusters, and no tracks

from the interaction point. Background is mainly from  $K_S \rightarrow \pi^0\pi^0$  events with two spurious clusters from splittings or accidental activity. Signal-event candidates are counted using the distribution in the plane of two  $\chi^2$ -like discriminating variables,  $\zeta_3$  and  $\zeta_2$ .  $\zeta_3$  is the quadratic sum of the residuals between the nominal  $\pi^0$  mass,  $m_{\pi^0}$ , and the invariant masses of three photon pairs formed from the six clusters present.  $\zeta_2$  is based on energy and momentum conservation in the  $\phi \rightarrow K_S K_L$ ,  $K_S \rightarrow \pi^0\pi^0$  decay hypothesis, as well as on the invariant masses of two photon pairs.  $\zeta_3$  and  $\zeta_2$  are evaluated with the most favorable cluster pairing in each case. Figure 8 shows the  $\zeta_2$  versus  $\zeta_3$  distributions obtained with  $450 \text{ pb}^{-1}$  of 2001–2002 data, as well as the predicted distribution from an MC sample with an effective statistics of 5.3 times that of the data. From the MC distribution, the number of predicted background counts is  $3.1 \pm 0.8 \pm 0.4$ ; two counts in the signal box are observed in data. KLOE thus obtains the 90% C.L. limit  $\text{BR} \leq 1.2 \times 10^{-7}$  (65), which is approximately a factor of six more stringent than the recent limit from NA48 (66). With the additional  $2 \text{ fb}^{-1}$  of data from 2004–2005 and improvements to the analysis under development, the KLOE limit can potentially be reduced by an additional order of magnitude.

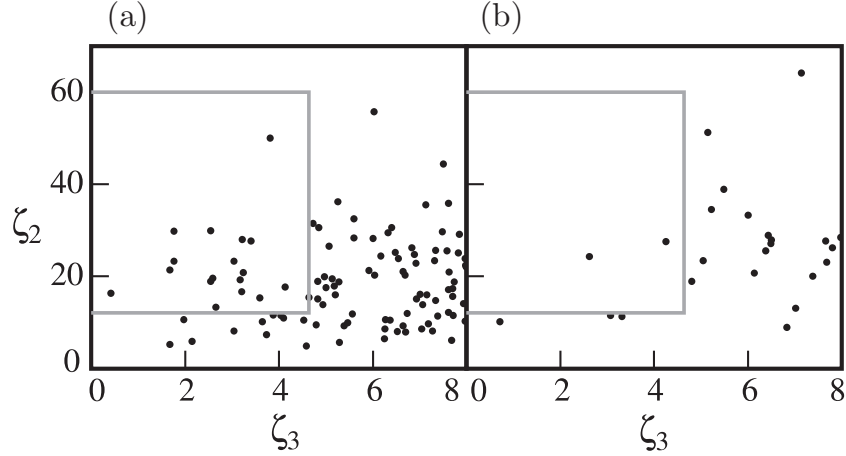


**Fig. 8.** Distribution of  $\zeta_2$  versus  $\zeta_3$  for candidate  $K_S \rightarrow 3\pi^0$  events: (a) from Monte Carlo simulation and (b) from  $450 \text{ pb}^{-1}$  of KLOE data.

#### 4.4 Charged Kaon Decays

The  $K^\pm \rightarrow \mu^\pm \nu$  ( $K_{\mu 2}$ ) decay represents approximately two-thirds of all  $K^\pm$  decays. It is often used as a reference for measuring other BRs, and, together with the  $K^\pm$  lifetime, provides a measurement of the decay constant  $f_K$ . The most recent measurement of  $\text{BR}(K_{\mu 2})$  is based on 62,000 events and dates back to 1972 (67). The stated error is  $\sim 0.7\%$ , with a  $0.4\%$  statistical contribution. It is important to improve the accuracy with which this BR is known.

The measurements of the  $K^\pm$  lifetime listed in the PDG compilation (52) exhibit poor consistency. The PDG fit has a confidence level of  $1.5 \times 10^{-3}$ , and the error on the recommended value is enlarged by a scale factor of 2.1. The dominant measurement, by Ott & Pritchard (68),  $\tau_{K^\pm} = 12.380 \pm 0.016 \text{ ns}$ , was obtained by combining the results from four runs. The systematic uncertainties for each of the individual runs are on the order of 27 ps, yet the overall systematic error is 14.7 ps. This is poorly explained. It is also curious that the stated fractional statistical error is  $0.63/\sqrt{N}$ , whereas from basic

statistical considerations, the fractional error must be at least  $1/\sqrt{N}$  (and should in fact be  $\sim 1.05/\sqrt{N}$  for a coverage of  $6\tau_{K^\pm}$ ). Thus, it is reasonable to be suspicious of the PDG value and its error. The measurement of the absolute  $K^\pm$  BRs and the  $K^\pm$  lifetime using tagged beams is an important part of the KLOE program.

**4.4.1  $K^+ \rightarrow \mu^+\nu(\gamma)$**  The KLOE measurement of this BR (69) is based on the use of  $K^- \rightarrow \mu^-\bar{\nu}$  decays for event tagging. Identification of a  $K^- \rightarrow \mu^-\bar{\nu}$  decay requires the presence of a two-track vertex in the DC. The nuclear interactions (NI) of the kaons affect the BR measurement, but not the tagging procedure. Because the nuclear cross section  $\sigma_{\text{NI}}(K^+) \approx 0.01\sigma_{\text{NI}}(K^-)$ , the use of a negative tag minimizes the corrections for NI. (The corrections are in fact negligible.) The large number of  $K_{\mu 2}$  decays allows for a statistical precision of  $\sim 0.1\%$ , while setting aside a generous sample for systematic studies.

As in the analysis of the  $K_L$  BRs, to avoid any bias due to differences in the  $K^-$  detection efficiency for different  $K^+$  decay modes, the decay products of the  $K^-$  must independently satisfy the trigger requirements. The tagging efficiency exhibits a small residual dependence on the  $K^+$  decay mode. This effect is corrected by MC simulation and checked using data.

$K^+ \rightarrow \mu^+\nu$  decays must have  $225 \leq p^* \leq 400$  MeV, where  $p^*$  is the momentum of the charged decay particle computed in the kaon rest frame assuming the pion mass. The true shape of the  $p^*$  distribution for signal events is obtained from a sample of control data. This distribution is used with the distributions for background sources to fit the  $p^*$  spectrum (Figure 9, center panel). Figure 9 (right panel) shows the spectrum after background subtraction. The shaded area is used to count  $K^+ \rightarrow \mu^+\nu$  events.

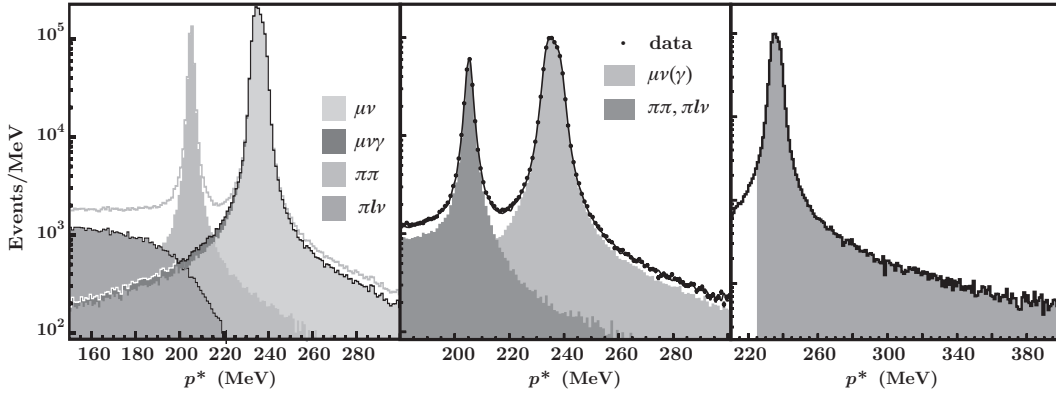


**Fig. 9.** (*Left panel*) Monte Carlo spectra of  $p^*$  for  $K^+$  decays, showing contributions from various channels. (*Center panel*) Distribution of  $p^*$  for  $\sim 60 \text{ pb}^{-1}$  of 2001–2002 KLOE data. (*Right panel*) Distribution of  $p^*$  after background subtraction. The shaded area is used to count  $K^+ \rightarrow \mu^+\nu$  events.

In a sample of four million tagged events, KLOE finds  $\sim 865,000$  signal events with  $225 \leq p^* \leq 400$  MeV, giving  $\text{BR}(K^+ \rightarrow \mu^+\nu(\gamma)) = 0.6366 \pm 0.0009 \pm 0.0015$ . This measurement is fully inclusive of final-state radiation (FSR) and has a 0.27% uncertainty.

**4.4.2 CHARGED KAON LIFETIME** This work is very near completion. We only mention that KLOE can measure the decay time for individual kaons in two ways. The first is to obtain the proper time from the kaon path length in the DC. The second is based on the precise measurement of the arrival times of the photons from  $K^\pm \rightarrow \pi^\pm \pi^0$  decays and the determination of the decay point from the track vertex in the DC. Both methods provide results accurate to the level of 0.1%.

**4.4.3 SEMILEPTONIC DECAYS OF CHARGED KAONS** Again the measurement is based on counting decays to each channel for samples of kaons tagged by detection of the two-body decay of the other kaon. After transforming to the center of mass of the tagging kaon,  $\mu\nu$  and  $\pi\pi^0$  decays are distinguished because  $p_\mu^* = 236$  MeV and  $p_\pi^* = 205$  MeV. Both types of decays are used as tags. The decay products of the tagging kaon must independently satisfy the trigger requirements. KLOE measures the semileptonic BRs separately for  $K^+$  and  $K^-$ . Therefore,  $\text{BR}(K^\pm \rightarrow \pi^0 e^\pm \nu(\gamma))$  and  $\text{BR}(K^\pm \rightarrow \pi^0 \mu^\pm \nu(\gamma))$  are each determined from four independent measurements ( $K^+$  and  $K^-$  decays;  $\mu\nu$  and  $\pi\pi^0$  tags). To identify signal events, two-body decays are first removed from the sample. The  $\gamma$ s from the  $\pi^0$  are then reconstructed and provide a measurement of the  $K^\pm$  decay time. Finally, the  $m_\ell^2$  distribution for the charged secondary lepton is reconstructed by TOF. After some further cleaning of the sample, the  $m_\ell^2$  distribution looks like that shown in Figure 10.

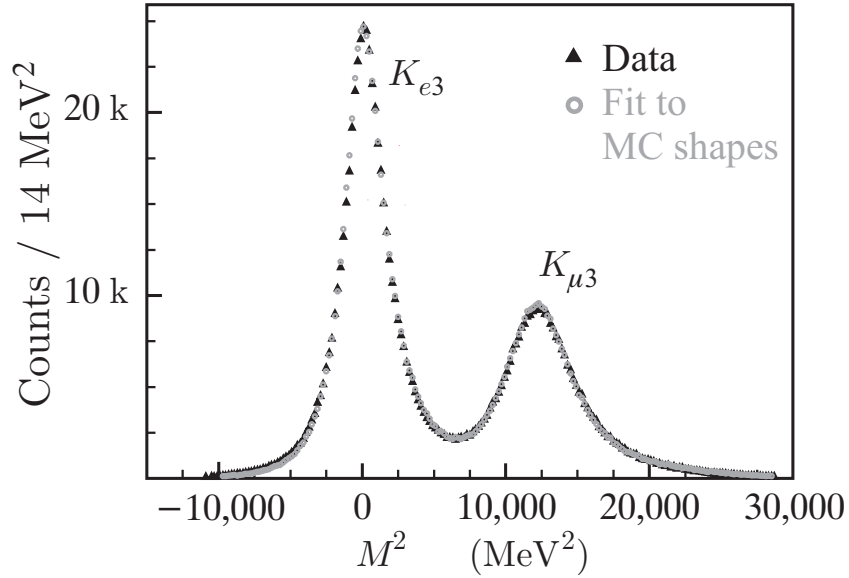


**Fig. 10.** Distribution of  $m_\ell^2$ , reconstructed using time-of-flight information, for events selected as  $K_{e3}^\pm$  decays. Also shown are the results of a fit to the Monte Carlo distributions for the two signal channels plus residual background.

The very good agreement of the four separate determinations of each BR is powerful proof of the validity of the analysis and provides an estimate of the systematic uncertainties. The KLOE values for the BRs are  $\text{BR}(K_{e3}^\pm) = (5.047 \pm 0.046_{\text{stat+tag}} \pm \sigma_{\text{syst}})\%$  and  $\text{BR}(K_{\mu3}^\pm) = (3.310 \pm 0.040_{\text{stat+tag}} \pm \sigma_{\text{syst}})\%$ . These values are averages over the four different samples for each channel and have been calculated with correlations carefully taken into account. These results were presented at the Lisbon European Physical Society conference (70) and are preliminary in the sense that a careful estimate of the systematic uncertainty on the signal selection efficiency is still in progress. We can however use the rms spread of the four measurements of each BR to estimate the systematic uncertainties at  $\sim 0.02\%$  absolute for both  $K_{e3}$  and  $K_{\mu3}$ , thus enlarging the errors stated above to  $0.05\%$  for both values. These results give  $R_{\mu e} \equiv \Gamma(K_{\mu3})/\Gamma(K_{e3}) = 0.656 \pm 0.008$ .

#### 4.5 KLOE, $V_{us}$ , and CKM Unitarity

As noted in Section 4.1.4, the KLOE data set on  $K_{\ell 3}$  decays allows multiple determinations of  $|V_{us}|$ , with very few external experimental inputs.

Following the derivation in Section 4.1.5, we compute the value of  $f_+^{K^0}(0)|V_{us}|$  from the decay rates for the five semileptonic decay processes measured by KLOE. For the moment, we use the values  $\lambda'_+ = 0.0221 \pm 0.0011$ ,  $\lambda''_+ = 0.0023 \pm 0.0004$ , and  $\lambda_0 = 0.0154 \pm 0.0008$ , obtained from a combined fit to  $K_{e3}$  and  $K_{\mu 3}$  results from KTeV (30) and ISTRA+ (31,32). We use the  $K_S$  and  $K^\pm$  lifetimes from the PDG (52). All BR measurements and the  $K_L$  lifetime value are from KLOE, as discussed in Sections 4.2 to 4.4. The input data and the results are collected in Table 4.

Table 4. Evaluation of  $f_+^{K^0}(0)|V_{us}|$  from KLOE data

Decay	BR <sup>a</sup>	$\tau^b$ (ns)	$\Gamma$ ( $\mu\text{s}^{-1}$ )	$f_+^{K^0}(0) V_{us} ^c$
$K_{Le3}$	0.4007(15) <sup>d</sup>	50.84(23)	7.88(4)	0.2164(6)
$K_{L\mu 3}$	0.2698(15)	50.84(23)	5.307(32)	0.2173(8)
$K_{Se3}$	$7.05(9) \times 10^{-4}$	0.08958(6)	7.87(10)	0.2161(14)
$K_{e3}^\pm$	0.0505(5)	12.385(25)	4.08(4)	0.2178(13)
$K_{\mu 3}^\pm$	0.0331(5)	12.385(25)	2.67(4)	0.2157(16)

<sup>a</sup>All branching ratios from KLOE.

<sup>b</sup> $K_L$  lifetime from KLOE;  $K_S$  and  $K^\pm$  lifetimes from PDG (52).

<sup>c</sup>Includes channel-specific  $SU(2)$  and electromagnetic corrections.

<sup>d</sup>Parentheses indicate errors on corresponding digits

Obviously, there are correlations between the different values for  $f_+^{K^0}(0)|V_{us}|$ , particularly for the case of  $K_{Le3}$  and  $K_{L\mu 3}$ , owing to the non-negligible error on the  $K_L$  lifetime ( $\sim 0.46\%$ ). With the correlations taken into account, we find

$$\langle f_+^{K^0}(0) \times |V_{us}| \rangle = 0.2167 \pm 0.0005 \quad (\text{or } \pm 0.23\%),$$

with  $\chi^2/\text{ndf} = 2.34/4$ . The quality of the fit is illustrated in Figure 11.

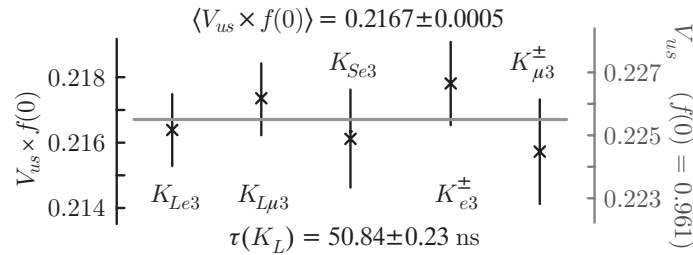


Fig. 11. Fit to the five KLOE values for  $f_+^{K^0}(0)|V_{us}|$ .

To extract the value of  $|V_{us}|$ , one needs an estimate of  $f_+^{K^0}(0)$ . Although the original calculation of Leutwyler & Roos (71) fell into disfavor a few years ago, it appears to have been confirmed recently by vastly improved lattice QCD calculations (72). Using  $f_+^{K^0}(0) = 0.961 \pm 0.008$  (71), we finally obtain

$$|V_{us}| = 0.2255 \pm 0.0019.$$

To test CKM unitarity, we use  $|V_{ud}| = 0.97377 \pm 0.00027$  (73). The first-row unitarity relation then gives

$$|V_{ud}|^2 + |V_{us}|^2 + |V_{ub}|^2 = 0.9738^2 + 0.2255^2 + \mathcal{O}(10^{-5}) = 0.9991 \pm 0.0010,$$

which is in good agreement with unitarity.

Measurements of the kaon system are very promising, and we believe that accuracies below the 0.1% level can be achieved. Experimental progress must be matched by better calculations, which lattice QCD seems close to attaining.

## 5 HADRONIC PHYSICS

A  $\phi$  factory such as DAΦNE is an ideal place at which to conduct a number of measurements in hadronic physics. The versatility of the KLOE experiment is well suited for such measurements.

The leptonic widths of the  $\phi$  meson provide a precise test of lepton universality. Interference between the continuum and  $\phi$ -mediated amplitudes leads to a modulation of the forward-backward asymmetry for  $e^+e^- \rightarrow e^+e^-$  events and of the cross section for  $e^+e^- \rightarrow \mu^+\mu^-$  events, providing sensitivity to  $\Gamma_{ee}$  and  $(\Gamma_{ee}\Gamma_{\mu\mu})^{1/2}$ , respectively. From a three-point scan about the  $\phi$  peak, conducted in 2002 (17.4 pb<sup>-1</sup> in total), KLOE obtains consistent values for the two quantities, from which  $\Gamma_{\ell\ell} = 1.320 \pm 0.023$  keV (46).

Radiative  $\phi$  decays ( $\phi \rightarrow \text{meson} + \gamma$ ) are unique probes of meson properties and structure. The transition rates are strongly dependent on the wave function of the final-state meson. They also depend on its flavor content, because the  $\phi$  is a nearly pure  $s\bar{s}$  state and because there is no photon-gluon coupling.

Finally, initial-state radiation (ISR) lowers the effective collision energy from  $\sqrt{s}$  to  $\sqrt{s_\pi} = (s - 2E_\gamma\sqrt{s})^{1/2}$ , providing access to hadronic states of mass  $\sqrt{s_\pi}$  from threshold to  $m_\phi$ . KLOE has exploited ISR to measure the  $e^+e^- \rightarrow \pi^+\pi^-$  cross section over this entire energy range without changing the DAΦNE energy.

### 5.1 Pseudoscalar Mesons: $\eta$ and $\eta'$

**5.1.1 THE  $\eta$  MESON** The BR for the decay  $\phi \rightarrow \eta\gamma$  is 1.3%. In 2.5 fb<sup>-1</sup> of KLOE data, there are 100 million  $\eta$  decays, identified clearly by their recoil against a photon of  $E = 363$  MeV.

Current results for  $m_\eta$  (74, 75) disagree at the  $8\sigma$  level. KLOE measures  $m_\eta$  using a kinematic fit to the  $\phi \rightarrow \eta\gamma \rightarrow 3\gamma$  topology. The absolute mass scale is determined by  $m_\phi$ . A preliminary analysis of the 2001–2002 data demonstrates that KLOE can measure  $m_\eta$  with competitive precision and can thereby clarify the current experimental situation.

Measurements of the Dalitz distributions for  $\eta \rightarrow 3\pi$  decays help in constraining calculations in chiral perturbation theory. These  $\Delta I = 1$  decays proceed primarily because of strong isospin breaking. As a result, once the phase-space integral in the amplitude for such decays is known, the widths give access to the ratio of quark masses  $(m_s^2 - \hat{m}^2)/(m_d^2 - m_u^2)$ , with  $\hat{m} = (m_u + m_d)/2$  (see References 77 and 78). In addition, the symmetries of the Dalitz plot for  $\eta \rightarrow \pi^+\pi^-\pi^0$  decays provide tests of charge-conjugation invariance. With the 2001–2002 data set, KLOE obtains a preliminary value for  $\alpha$ , the Dalitz-plot slope in  $\eta \rightarrow 3\pi^0$  decays, that is competitive in precision to that from the Crystal Ball experiment (79), as well as limits on the left-right, quadrant, and sextant asymmetries in the Dalitz plot for  $\eta \rightarrow \pi^+\pi^-\pi^0$  decays significantly more stringent than the current PDG values (52).



The decay  $\eta \rightarrow \pi^0 \gamma \gamma$  is particularly interesting in chiral perturbation theory. As noted in Reference 80, there is no  $\mathcal{O}(p^2)$  contribution, and the  $\mathcal{O}(p^4)$  contribution is small.<sup>3</sup> The experimental value of the decay rate offers a point of comparison for third-order chiral perturbation theory calculations. The history of attempts to measure the rate for this decay is confused owing to persistent problems with background, in particular from  $\eta \rightarrow 3\pi^0$ . In both existing plausible BR measurements,  $\eta$  mesons were produced via the reaction  $\pi^- p \rightarrow \eta n$  (81, 82). Only the result from the Crystal Ball (82) is in agreement with chiral perturbation theory predictions. At KLOE, the decay can be reconstructed with full kinematic closure and without complications from certain backgrounds present in fixed-target experiments, such as  $\pi^- p \rightarrow \pi^0 \pi^0 n$ . Using the 2001–2002 data set, KLOE has obtained the preliminary result  $\text{BR}(\eta \rightarrow \pi^0 \gamma \gamma) = (8.4 \pm 2.7 \pm 1.4) \times 10^{-5}$ . This result is approximately a factor of four lower than that from the Crystal Ball. It is in agreement with the results of  $\mathcal{O}(p^6)$  tree-level chiral perturbation theory calculations reported in References 80 and 83 and with the  $\mathcal{O}(p^6)$  Nambu–Jona-Lasinio model calculation of Reference 84.

The decay  $\eta \rightarrow 3\gamma$  violates  $C$ , while the decay  $\eta \rightarrow \pi^+ \pi^-$  violates both  $P$  and  $CP$ . The Standard Model cannot accommodate either decay at any currently observable level. KLOE has conducted a search for the decay  $\eta \rightarrow 3\gamma$  using 410 pb<sup>-1</sup> of the 2001–2002 data (85). A clean sample of 4 $\gamma$  events is first isolated. Events with  $\phi \rightarrow \eta \gamma$  and  $\eta \rightarrow 3\gamma$  would be distinguished by the characteristic energy of the radiated photon ( $E_{\text{rad}} = 363$  MeV), which in most cases would also be the most energetic photon in the event. No peak is observed in the distribution of the maximum photon energy for 4 $\gamma$  events. KLOE obtains the limit  $\text{BR}(\eta \rightarrow 3\gamma) \leq 1.6 \times 10^{-5}$  at 90% C.L., the most stringent obtained to date. KLOE has also searched for evidence of the decay  $\eta \rightarrow \pi^+ \pi^-$  in the tail of the  $M_{\pi\pi}$  distribution for  $e^+ e^- \rightarrow \pi^+ \pi^- \gamma$  events in which the photon is emitted at large polar angles ( $\theta > 45^\circ$ ). 350 pb<sup>-1</sup> of 2001–2002 data were analyzed as described in Section 5.2. No peak is observed in the distribution of  $M_{\pi\pi}$  in the vicinity of  $m_\eta$ . The corresponding limit is  $\text{BR}(\eta \rightarrow \pi^+ \pi^-) \leq 1.3 \times 10^{-5}$  at 90% C.L. (86), which is more stringent than the previous limit by a factor of 25.

**5.1.2 THE  $\eta'$  MESON** The magnitude of  $\text{BR}(\phi \rightarrow \eta' \gamma)$  is a probe of the  $s\bar{s}$  content of the  $\eta'$  (87). The ratio  $R_{\eta'} \equiv \text{BR}(\phi \rightarrow \eta' \gamma) / \text{BR}(\phi \rightarrow \eta \gamma)$  can be related to the pseudoscalar mixing angle  $\varphi_P$  in the basis  $\{|u\bar{u} + d\bar{d}\rangle / \sqrt{2}, |s\bar{s}\rangle\}$ , offering an important point of comparison for the description of the  $\eta$ - $\eta'$  mixing in extended chiral perturbation theory (88). At KLOE, the  $\phi \rightarrow \eta' \gamma$  decay is identified in the channel in which  $\eta' \rightarrow \eta \pi^+ \pi^-$  and  $\eta \rightarrow \gamma \gamma$ , whereas the  $\phi \rightarrow \eta \gamma$  decay is identified in the channel in which  $\eta \rightarrow \pi^+ \pi^- \pi^0$ . In either case, the final state contains a  $\pi^+$ , a  $\pi^-$ , and three photons. As a result, many systematics cancel in the measurement of  $R_{\eta'}$ .

A first KLOE measurement of this ratio was conducted using 16 pb<sup>-1</sup> of data from the year 2000 (89). The value obtained was  $R_{\eta'} = (4.70 \pm 0.47 \pm 0.31) \times 10^{-3}$ . This allows  $\varphi_P$  to be determined to better than 2° using relations in References 88 and 90. Together with additional constraints from the rates for  $\eta'$  decays into  $\rho \gamma$  and  $\gamma \gamma$ , which give information about the nonstrange quark content of the  $\eta'$ , the KLOE result for  $\varphi_P$  can be used to place a limit on the gluonium content of the  $\eta'$ . With  $|\eta'\rangle = X_{\eta'} |u\bar{u} + d\bar{d}\rangle / \sqrt{2} + Y_{\eta'} |s\bar{s}\rangle + Z_{\eta'} |gg\rangle$ , where the last term represents the possible gluonium content of the  $\eta'$  meson, the above considerations give  $Z_{\eta'}^2 = 0.06_{-0.06}^{+0.09}$ , which is compatible with zero.

A recent extension of this analysis is based on the identification of the  $\pi^+ \pi^- 7\gamma$  final

<sup>3</sup>We recall that in chiral perturbation theory, the effective Lagrangian is expanded in a series of terms with increasing numbers of field derivatives and quark mass terms, and that the chiral orders in the meson sector are always even.



state (i.e.,  $\eta' \rightarrow \eta\pi^+\pi^-$  with  $\eta \rightarrow 3\pi^0$ , or  $\eta' \rightarrow \eta\pi^0\pi^0$  with  $\eta \rightarrow \pi^+\pi^-\pi^0$ ). A preliminary result based on the analysis of the full 2001–2002 data set gives  $R_{\eta'}$  with a total error of approximately 4.5%. Uncertainties in the intermediate  $\eta'$  BRs dominate this error. KLOE can improve the knowledge of these BRs by using the recently acquired data.

## 5.2 Scalar Mesons: $f_0(980)$ and $a_0(980)$

The compositions of the five scalar mesons with masses below 1 GeV are not well understood. Of these, the well-established states are the  $I = 0$   $f_0(980)$  and the  $I = 1$   $a_0(980)$ . Together with the very broad  $I = 0$   $f_0(400\text{--}1200)$  ( $\sigma$ ) and possible  $I = 1/2$   $K_0^*(800)$  ( $\kappa$ ) states, these may be grouped into a nonet with an inverted mass structure. Both the low masses of these mesons as a whole and this inverted mass structure are explained by the hypothesis that these are not conventional  $q\bar{q}$  mesons, but are in fact  $qq\bar{q}\bar{q}$  states (91). In this case, the mass degeneracy of the  $f_0$  and  $a_0$  is explained by the fact that they contain “hidden”  $s\bar{s}$  pairs, whereas the  $\sigma$ , the state of lowest mass, is  $u\bar{d}d\bar{u}$ . The quarks and antiquarks may also be paired into two pseudoscalar mesons (92). In this case, the  $f_0$  and  $a_0$  are interpreted as  $K\bar{K}$  “molecules.” The proximity of the  $f_0$  and  $a_0$  to the  $K\bar{K}$  thresholds, together with the fact that these states are strongly coupled to  $K\bar{K}$ , suggests that the  $f_0$  and  $a_0$  must in any case be surrounded by a cloud of virtual  $K\bar{K}$  pairs (93). Alternatively, there are unitarized quark models in which both the light and heavy scalars are understood as dynamically generated states “seeded” by bare  $q\bar{q}$  states (see, e.g., Reference 94).

Decays such as  $\phi \rightarrow f_0\gamma \rightarrow \pi\pi\gamma$  and  $\phi \rightarrow a_0\gamma \rightarrow \eta\pi^0\gamma$  are suppressed unless the  $f_0$  and  $a_0$  have significant  $s\bar{s}$  content. The BRs for these decays are estimated to be on the order of  $10^{-4}$  if the  $f_0$  and  $a_0$  are  $qq\bar{q}\bar{q}$  states (in which case they contain an  $s\bar{s}$  pair), or on the order of  $10^{-5}$  if the  $f_0$  and  $a_0$  are conventional  $q\bar{q}$  states (95,96). If the  $f_0$  and  $a_0$  are  $K\bar{K}$  molecules, the BR estimates are sensitive to assumptions about the spatial extension of these states (97).

Apart from the BRs for these decays, the analysis of the  $\pi\pi$  and  $\eta\pi^0$  invariant-mass distributions can shed light on the nature of the  $f_0$  and  $a_0$  because fits to the distributions provide estimates of the couplings of these mesons to the  $\phi$  and/or to the final-state particles. The fit to the two-pion invariant-mass ( $M_{\pi\pi}$ ) distribution for  $\phi \rightarrow \pi\pi\gamma$  decays may also provide evidence of a contribution from the  $\sigma$ . Such fits necessarily assume a specific model for the decay mechanism. Because of the proximity of the  $f_0$  and  $a_0$  masses to the  $K\bar{K}$  threshold, and because these mesons are known to couple strongly to  $K\bar{K}$ , the kaon-loop model (Figure 12, left panel) is often used (95).

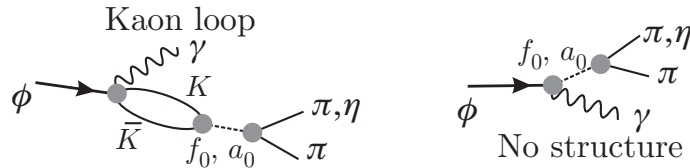


**Fig. 12.** Amplitudes used to compute the  $\pi\pi$  and  $\eta\pi^0$  mass spectra for  $\phi \rightarrow S\gamma$ .

The expression for the rate for E1  $\phi \rightarrow S\gamma$  transitions ( $S = f_0$  or  $a_0$ ) contains a factor  $E_\gamma^3$  (where  $E_\gamma$  is the energy of the radiated photon), as required by considerations of phase space and gauge invariance. As a result, the invariant-mass distributions in  $\phi \rightarrow S\gamma$  decays are cut off above  $m_\phi$  and develop a long tail toward lower mass values. The fit results therefore depend strongly on the scalar meson masses and widths.

5.2.1  $\phi \rightarrow \pi^0\pi^0\gamma$  AND  $\phi \rightarrow \eta\pi^0\gamma$  The first KLOE studies of the decays  $\phi \rightarrow \pi^0\pi^0\gamma$  (98) and  $\phi \rightarrow \eta\pi^0\gamma$  (99) were performed with the  $17 \text{ pb}^{-1}$  of data collected in 2000.

Amplitudes contributing to  $\phi \rightarrow \pi^0\pi^0\gamma$  include  $\phi \rightarrow S\gamma$  (with  $S = f_0$  or  $\sigma$ ) and  $\phi \rightarrow \rho^0\pi^0$  (with  $\rho^0 \rightarrow \pi^0\gamma$ ). The  $M_{\pi\pi}$  distribution was fit with a function including terms describing the contribution from  $\phi \rightarrow S\gamma$ , that from  $\phi \rightarrow \rho\pi$ , and their interference. Two forms for the  $\phi \rightarrow S\gamma$  term were used: one including only the process  $\phi \rightarrow f_0\gamma$  represented by the kaon-loop diagram of Figure 12 (95), and one including an additional contribution from  $\phi \rightarrow \sigma\gamma$ , represented by a point-like coupling. The free parameters in the fits describing the scalars were  $m_{f_0}$ , the coupling constants  $g_{f_0K^+K^-}$  and  $g_{f_0\pi^+\pi^-}$  for the kaon loop, and, in the fit including the  $\sigma$ , the coupling  $g_{\phi\sigma\gamma}$ . The fits gave negligibly small contributions from the  $\rho\pi$  and associated interference terms. The fit including the  $\sigma$  gave a significantly better value of  $\chi^2/\text{ndf}$ . The value obtained for  $\text{BR}(\phi \rightarrow \pi^0\pi^0\gamma)$  was  $(1.09 \pm 0.03 \pm 0.05) \times 10^{-4}$ , in good agreement with the results from the CMD-2 (100) and SND (101) experiments at the VEPP-2M collider in Novosibirsk, and significantly more precise.

The  $\phi \rightarrow \eta\pi^0\gamma$  channel is simpler to treat in that there is no contribution from the  $\sigma$ . The amplitudes contributing are  $\phi \rightarrow a_0\gamma$  and  $\phi \rightarrow \rho^0\pi^0$ , with  $\rho^0 \rightarrow \eta\gamma$ . In the KLOE analysis, final states corresponding to two different  $\eta$  decay channels were studied:  $\eta \rightarrow \gamma\gamma$  ( $5\gamma$  final state) and  $\eta \rightarrow \pi^+\pi^-\pi^0$  ( $\pi^+\pi^-5\gamma$  final state). The  $M_{\eta\pi}$  distributions for each sample were fit simultaneously with a function analogous to that discussed above. The fit parameters describing the  $a_0$  were the coupling constants  $g_{a_0K^+K^-}$  and  $g_{a_0\eta\pi^0}$ ; the mass of the  $a_0$  was fixed to the PDG value (52). The fit gave a contribution from the  $\rho\pi$  term consistent with zero. The values obtained for  $\text{BR}(\phi \rightarrow \eta\pi^0\gamma)$  using the  $5\gamma$  and  $\pi^+\pi^-5\gamma$  samples were  $(8.51 \pm 0.51 \pm 0.57) \times 10^{-5}$  and  $(7.96 \pm 0.60 \pm 0.40) \times 10^{-5}$ , respectively. These two values are in agreement with each other and with the results from CMD-2 (100) and SND (102); again, the KLOE data substantially improve the knowledge of these BRs.

In either case, the good quality of the fit establishes that the kaon-loop model provides a valid description of the decay process. The BRs for  $\phi \rightarrow f_0\gamma$  and  $\phi \rightarrow a_0\gamma$  were obtained by integrating the appropriate terms of the fit functions. Assuming dominance of the  $\pi\pi$  and  $\eta\pi^0$  channels in  $f_0$  and  $a_0$  decays and that  $\text{BR}(f_0 \rightarrow \pi^+\pi^-) = 2 \text{BR}(f_0 \rightarrow \pi^0\pi^0)$ , the values  $\text{BR}(\phi \rightarrow f_0\gamma) = (4.47 \pm 0.21) \times 10^{-4}$  and  $\text{BR}(\phi \rightarrow a_0\gamma) = (0.74 \pm 0.07) \times 10^{-4}$  are obtained. These BRs are large, as are the values obtained for the couplings of the scalars to  $K\bar{K}$ , especially for the  $f_0$ . These results have been interpreted to support the hypothesis that the  $f_0$  and  $a_0$  consist of a compact  $qq\bar{q}\bar{q}$  core surrounded by a virtual  $K\bar{K}$  cloud (103). Various interpretations of the KLOE data exist, however, and the data have been reanalyzed by many authors (104,105,106). Although these authors obtain different results for  $\text{BR}(\phi \rightarrow f_0\gamma)$  and the various couplings, in general they find support for the  $qq\bar{q}\bar{q}$  or  $K\bar{K}$  hypotheses in the KLOE data. One reanalysis that arrives at a different conclusion is that of Boglione & Pennington (107). They perform a  $T$ -matrix  $\pi\pi$ - $K\bar{K}$  coupled-channel analysis of the data on  $\phi \rightarrow \pi^0\pi^0\gamma$  from KLOE and SND, and obtain  $\text{BR}(\phi \rightarrow f_0\gamma) = 3.4 \times 10^{-5}$ , which is smaller than the KLOE fit result by an order of magnitude. They argue that, notwithstanding the large  $\phi \rightarrow K\bar{K}$  coupling, the low-mass enhancement from gauge invariance increases the importance of the  $\phi \rightarrow \pi\pi\gamma$  coupling followed by  $\pi\pi \rightarrow \pi\pi$  rescattering. Thus, approximately 90% of the observed  $\phi \rightarrow \pi^0\pi^0\gamma$  width is from decay through the  $\sigma$ , rather than through the  $f_0$ .

The analyses of the  $\phi \rightarrow \pi^0\pi^0\gamma$  and  $\phi \rightarrow \eta\pi^0\gamma$  decays based on the 2001–2002 data set benefit from an increase in statistics by a factor of  $\sim 30$  and are nearing completion. Fits using two models are under development: an implementation of the kaon-loop model embodying some of the extensions of Reference 106, and the no-structure model (108) illustrated in Figure 12 (right panel). In this latter model, the scalar is described by a

Breit-Wigner amplitude with a mass-dependent width; the free parameters of the fit are  $m_{f_0}$  and the couplings  $g_{\phi S\gamma}$ ,  $g_{f_0\pi\pi}$  or  $g_{a_0\eta\pi}$ , and  $g_{SK\bar{K}}$  (109). The fit includes two additional complex parameters to describe contributions to the amplitude from background processes.

**5.2.2  $\phi \rightarrow \pi^+\pi^-\gamma$**  KLOE has recently published a study of the decay  $\phi \rightarrow f_0\gamma \rightarrow \pi^+\pi^-\gamma$  based on the 2001–2002 data set (110). Only a small fraction of the  $e^+e^- \rightarrow \pi^+\pi^-\gamma$  events involve the  $f_0$ ; the principal contributions are from events in which the photon is from ISR or FSR. At large values of the photon polar angle  $\theta_\gamma$ , the ISR contribution is strongly reduced; the analysis is performed on the  $M_{\pi\pi}$  distribution for events with  $\theta_\gamma > 45^\circ$ . The  $M_{\pi\pi}$  distribution is fit with a function consisting of the terms

$$\frac{d\sigma}{dM_{\pi\pi}} = \frac{d\sigma_{\text{ISR}}}{dM_{\pi\pi}} + \frac{d\sigma_{\text{FSR}}}{dM_{\pi\pi}} + \frac{d\sigma_{\rho\pi}}{dM_{\pi\pi}} + \frac{d\sigma_{S\gamma}}{dM_{\pi\pi}} \pm \frac{d\sigma_{\text{int}}}{dM_{\pi\pi}}.$$

Analytic expressions for the ISR, FSR, and  $\rho\pi$  ( $e^+e^- \rightarrow \rho^\pm\pi^\mp$ ,  $\rho^\pm \rightarrow \pi^\pm\gamma$ ) terms are taken from References 96 and 111. The last two terms describe the decay  $\phi \rightarrow S\gamma \rightarrow \pi\pi\gamma$  and its interference with FSR; the interference may be constructive or destructive. The  $M_{\pi\pi}$  distribution has been fit using expressions for the scalar-mediated amplitude obtained from the kaon-loop model, the no-structure model, and the  $T$ -matrix coupled-channel framework. Figure 13 (left panel) shows the  $M_{\pi\pi}$  distribution, with the result of the kaon-loop fit superimposed. The overall appearance of the distribution is dominated by the radiative return to the  $\rho$ ; the  $f_0$  appears as the peak-like structure in the region 900–1000 MeV. Figure 13 (right panel) shows the data in this mass region, with the ISR, FSR, and  $\rho\pi$  terms subtracted.

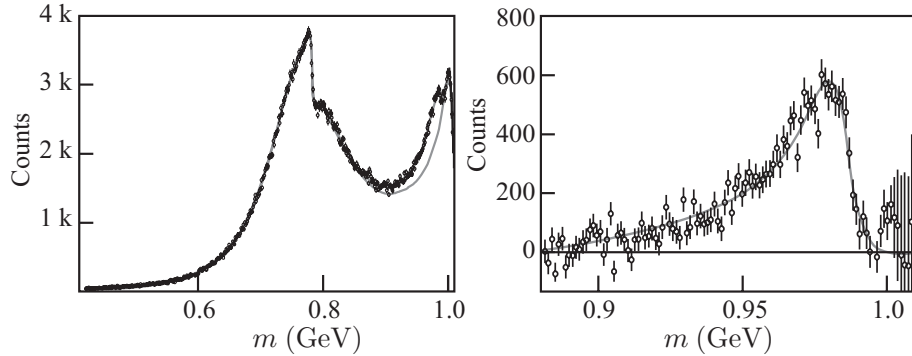


**Fig. 13.** (*Left panel*)  $M_{\pi\pi}$  distribution for large-photon-angle  $\pi^+\pi^-\gamma$  events from 2001–2002 KLOE data. Fits with and without the  $f_0$  contribution are shown. (*Right panel*) Distribution in the region of the  $f_0$ , with the initial-state radiation, final-state radiation, and  $\rho\pi$  contributions subtracted.

Both the kaon-loop and no-structure fits strongly prefer destructive interference between the  $S\gamma$  and FSR amplitudes, which damps the low-mass tail of the  $f_0$ . No improvement in the quality of the kaon-loop fit is observed when the  $\sigma$  is included. Both fits give values for  $m_{f_0}$  in agreement with the PDG estimate (52). Large discrepancies between the kaon-loop and no-structure values are obtained for the couplings  $g_{f_0 K^+ K^-}$  and  $g_{f_0 \pi^+ \pi^-}$ . The kaon-loop fit gives coupling values in reasonable agreement with those obtained from the fit to the KLOE  $\phi \rightarrow \pi^0 \pi^0 \gamma$  data discussed above. Both fits give  $g_{f_0 K^+ K^-}^2 / g_{f_0 \pi^+ \pi^-}^2 \approx 3$ , which indicates that the  $f_0$  couples more strongly to kaons than to pions. Integrating the appropriate terms of the fit functions gives values for  $\text{BR}(\phi \rightarrow f_0 \gamma)$  in the neighborhood of  $3 \times 10^{-4}$ .

### 5.3 The Hadronic Cross Section and $a_\mu$

**5.3.1 THE MUON ANOMALY  $a_\mu$**  The observation of the anomalous magnetic moment of the electron helped drive the development of quantum electrodynamics (QED). The value of the muon anomaly,  $a_\mu$ , is  $(m_\mu/m_e)^2 \approx 40,000$  times more sensitive than that of the electron to high-mass states in the polarization of the vacuum. The Muon  $g - 2$  Collaboration (E821) at Brookhaven has used stored muons to measure  $a_\mu$  to 0.5 ppm (112):

$$a_\mu = \frac{g_\mu - 2}{2} = (116,592,080 \pm 60) \times 10^{-11}.$$

The muon anomaly receives contributions from QED, weak, and hadronic loops in the photon propagator, as well as from light-by-light scattering. The lowest-order hadronic contribution is  $a_\mu^{\text{had}} = \sim 7000 \times 10^{-11}$ , with an uncertainty of  $\sim 60 \times 10^{-11}$ . To the extent that this uncertainty can be reduced, the E821 measurement offers a potential probe of new physics at TeV energy scales.

The low-energy contribution to  $a_\mu^{\text{had}}$  cannot be obtained from perturbative QCD. It has often been calculated from measurements of the cross section for  $e^+e^-$  annihilation into hadrons via the dispersion integral

$$a_\mu^{\text{had}} = \frac{1}{4\pi^3} \sum_f \int_{s_{\text{th}}(f)}^{\infty} K(s) \sigma(e^+e^- \rightarrow f) ds,$$

where  $K(s)$ , the QED kernel, is a monotonic function that varies approximately as  $1/s$ , with  $s$  the squared center-of-mass collision energy. This amplifies the importance of the cross-section measurements at low energy. Approximately two-thirds of the integral is contributed by the process  $e^+e^- \rightarrow \pi^+\pi^-$  for  $\sqrt{s} < 1$  GeV, i.e., in the vicinity of  $m_\rho$ . Before the arrival of the KLOE results we discuss below, calculations of  $a_\mu^{\text{had}}$  from world  $e^+e^-$  data (dominated at low energies by the CMD-2 measurement of Reference 113) led to a value of  $a_\mu \sim 2.4\sigma$  lower (114) than the final value reported by E821.

Assuming the validity of the conserved-vector-current hypothesis, the  $e^+e^-$  cross section for the production of a neutral hadronic state  $f^0$  can also be obtained from the spectral function for the decay of the  $\tau$  lepton to the hadronic state  $f^-$ , where  $f^0$  and  $f^-$  are connected by an isospin rotation. (The spectral function for  $\tau^- \rightarrow f^- \nu_\tau$  decay is obtained from  $d\text{BR}(\tau^- \rightarrow f^- \nu_\tau)/ds$ , with  $s$  as the squared mass of the state  $f^-$ .) With  $f^0 = \pi^+\pi^-$  and  $f^- = \pi^-\pi^0$ , one obtains the  $I = 1$  contribution to  $\sigma_{\pi^+\pi^-}$ . A recent evaluation (115) of  $a_\mu^{\text{had}}$  based on  $\tau$  data rather than on  $e^+e^-$  data at low energies gives a value for  $a_\mu$  that is only  $(76 \pm 90) \times 10^{-11}$  ( $0.8\sigma$ ) lower than the final E821 value (114). Thus, even before KLOE results became available, there was some discrepancy between  $e^+e^-$ - and  $\tau$ -based evaluations of  $a_\mu$ . We return to this point in Section 5.3.3.

**5.3.2 MEASUREMENT OF  $\sigma_{\pi^+\pi^-}$  AT KLOE** DAΦNE is highly optimized for running at  $\sqrt{s} = m_\phi$ ;  $\sqrt{s}$  cannot be varied over a broad range. However, ISR naturally provides access, via the process  $e^+e^- \rightarrow \pi^+\pi^-\gamma$ , to hadronic states of lower mass. The cross section  $\sigma_{\pi^+\pi^-}$  over the entire interval from threshold to  $m_\phi$  is reflected in the distribution of  $s_\pi = M_{\pi\pi}^2$  for  $\pi^+\pi^-\gamma$  events,

$$\sigma_{\pi^+\pi^-}(s_\pi) = \frac{s_\pi}{H(s_\pi|s)} \left. \frac{d\sigma_{\pi^+\pi^-\gamma}}{ds_\pi} \right|_{\text{ISR}}, \quad (13)$$

where  $H$ , the “radiator function,” describes the ISR spectrum. Note the subscript ISR on the differential  $\pi^+\pi^-\gamma$  cross section. This is very important because the contribution from FSR is of the same order as that from the ISR process.

To correctly calculate  $H$  and estimate the effects of FSR, an accurate simulation is critical. The KLOE analysis is based on the PHOKHARA event generator (116), which includes next-to-leading-order ISR (two initial-state photons) and has a stated accuracy of 0.5%. Leading-order FSR and ISR-FSR terms are also included. In particular, ISR-FSR events are related to virtual  $\pi^+\pi^-\gamma$  states in the photon propagator and require special treatment to be fully counted in the evaluation of  $a_\mu^{\text{had}}$ .

At small photon polar angle  $\theta_\gamma$ , ISR events are vastly more abundant than FSR events. Requiring angular separation between the pions and the photon further suppresses FSR (117). For these reasons, the first KLOE measurement (118) was performed using events with  $\theta_\gamma < 15^\circ$  and  $\theta_\pi > 50^\circ$  for both pion tracks. In such events, the photon is lost down the beam pipe;  $s_\pi$  is computed from the pion momenta. These fiducial cuts additionally reduce background from  $\phi \rightarrow \pi^+\pi^-\pi^0$  and  $\phi \rightarrow f_0\gamma \rightarrow \pi^+\pi^-\gamma$  events (see Section 5.2.2). They also limit the accessible range in  $s_\pi$ , because in  $\pi^+\pi^-\gamma$  events with a hard photon emitted at small angle, one or both pions from the low-mass  $\pi^+\pi^-$  pair do not enter the tracking volume.

The KLOE results obtained with 141 pb<sup>-1</sup> of 2001 data (118) are summarized in Figure 14. The left panel shows the measurement of  $d\sigma_{\pi^+\pi^-\gamma}/ds_\pi$ .

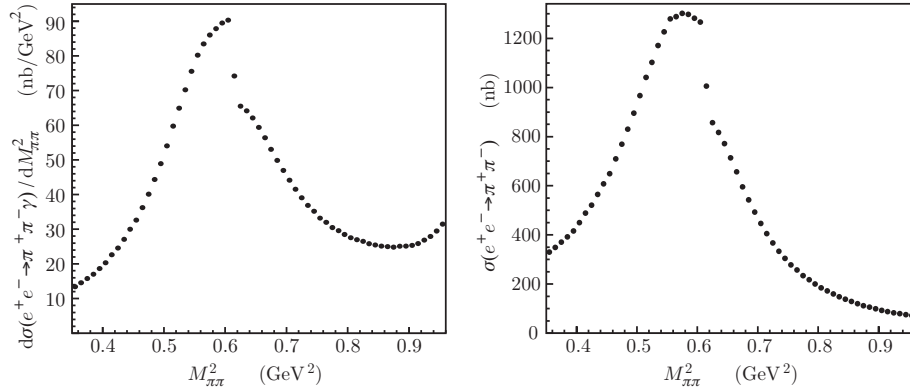


**Fig. 14.** (Left panel) KLOE measurement of  $d\sigma_{\pi^+\pi^-\gamma}/ds_\pi$ . (Right panel) The cross section  $\sigma_{\pi^+\pi^-}$ , including final-state radiation and without correction for vacuum polarization.

The statistical errors range from  $\sim 2\%$  at the lower limit in  $s_\pi$  to  $\sim 0.5\%$  at the  $\rho$  peak. The experimental systematic uncertainties are mostly flat in  $s_\pi$  and amount to 0.9%. The luminosity was estimated using large-angle Bhabha scattering and contributes an additional, dominantly theoretical uncertainty of 0.6%. The right panel of Figure 14 shows the cross section  $\sigma_{\pi^+\pi^-}$  evaluated via Equation 13. The contribution to the systematic uncertainty on  $\sigma_{\pi^+\pi^-}$  from FSR is 0.3%, whereas that from the accuracy of  $H$  is 0.5%. Finally, for the evaluation of  $a_\mu^{\text{had}}$ , it is necessary to remove the effects of vacuum polarization in the photon propagator for the process  $e^+e^- \rightarrow \pi^+\pi^-$  itself by correcting for the running of  $\alpha_{\text{em}}$ . This contributes 0.2% to the systematic uncertainty.

For the contribution to  $a_\mu^{\pi\pi}$  from the energy interval  $0.35 < s < 0.95$  GeV<sup>2</sup>, KLOE obtains

$$a_\mu^{\pi\pi}(0.35 < s < 0.95 \text{ GeV}^2) = (3887 \pm 8_{\text{stat}} \pm 35_{\text{syst}} \pm 35_{\text{th}}) \times 10^{-11}.$$

As a point of comparison, KLOE has evaluated the contribution to  $a_\mu^{\pi\pi}$  for the energy interval covered by CMD-2 ( $0.37 < s < 0.93$  GeV<sup>2</sup>). The results from the two experiments

differ by only  $30 \times 10^{-11}$  ( $0.5\sigma$ ). Inclusion of the KLOE data together with the CMD-2 data in the evaluation of  $a_\mu^{\text{had}}$  increases the discrepancy between the calculated and measured values of  $a_\mu$  to  $(252 \pm 92) \times 10^{-11}$  ( $\sim 2.7\sigma$ ) (119).

**5.3.3 COMPARISON OF  $e^+e^-$  AND  $\tau$  DATA** As noted at the end of Section 5.3.1,  $e^+e^-$ - and  $\tau$ -based evaluations of  $a_\mu^{\text{had}}$  give different results. The KLOE data increase this discrepancy, whereas new data from SND (120) decrease it. Figure 15 compares evaluations of the pion form factor from  $\tau$  and  $e^+e^-$  data by Davier et al. (121). The KLOE data clearly exhibit a trend that is systematically different from that of the  $\tau$  data. The SND points conform more closely to the  $\tau$  data, whereas the CMD-2 points lie somewhere in between. As a gauge of the significance of these trends, Davier et al. have evaluated  $\text{BR}(\tau^- \rightarrow \pi^- \pi^0 \nu_\tau)$  from the cross-section data of each of the three experiments. The BR values calculated from the KLOE and CMD-2 data are  $3.8\sigma$  and  $3.1\sigma$  lower than the measured value, respectively, and are reasonably compatible with each other. The BR value from the SND data is compatible with ( $0.9\sigma$  lower than) the measured value.

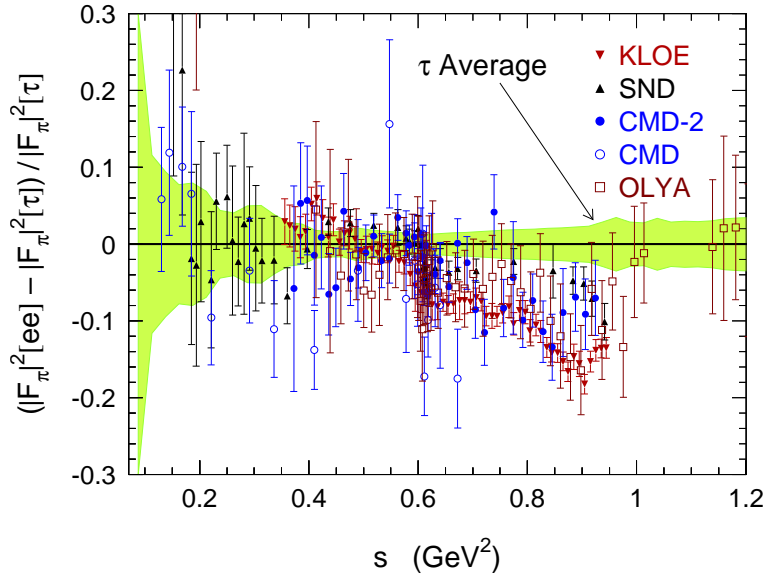


**Fig. 15.** Relative difference between the pion form factor  $|F_\pi(s)|^2$  as evaluated from  $\tau$  spectral functions (*band shows error*), and  $\sigma_{\pi^+\pi^-}$  measurements from various  $e^+e^-$  experiments (*points*). Reprinted figure with permission from M. Davier, A. Höcker, Z. Zhang, *Rev. Mod. Phys.*, accepted for publication (121). In press by the American Physical Society.

Questions about possible biases in the results of any of the three experiments may be resolved by new data and by analysis improvements. CMD-2 has recently announced preliminary results from the analysis of their 1996–2000 data for the entire interval in  $\sqrt{s}$  from threshold to 1.4 GeV, including a nearly 10-fold increase in statistics in the region covered by their previous measurement (122). KLOE prospects are discussed below.

**5.3.4 FORTHCOMING IMPROVEMENTS WITH KLOE** KLOE is actively working on repeating the small-photon-angle measurement described above using data from 2002–2005 and a series of improvements to the reconstruction and analysis.

The contribution to  $a_\mu^{\text{had}}$  from  $e^+e^- \rightarrow \pi^+\pi^-$  in the interval in  $s$  between threshold and  $0.35 \text{ GeV}^2$  is approximately  $1000 \times 10^{-11}$ . As noted above, the fiducial cuts implemented in the KLOE measurement restrict the acceptance to higher values of  $M_{\pi\pi}$ . To explore the



low-mass part of the spectrum, KLOE must accept events with  $\theta_\gamma > 40^\circ$ . Background from  $\phi \rightarrow \pi^+\pi^-\pi^0$  events can be rejected by kinematic closure if explicit detection of the photon from  $\pi^+\pi^-\gamma$  is required. FSR is a more complicated problem: For  $\theta_\gamma > 40^\circ$ , ISR and FSR events contribute nearly equally to the  $\pi^+\pi^-\gamma$  spectrum in the tails of the  $\rho$ , and the accuracy of the generator used to obtain FSR corrections is critical. As discussed by Binner et al. (117), the ISR-FSR interference results in a measurable charge asymmetry, which is a useful gauge of the accuracy of the simulation. KLOE has performed comparisons of this type for the analysis of  $\phi \rightarrow \pi^+\pi^-\gamma$  discussed in Section 5.2.2 (110). Moreover, with the full statistics of the complete data set, KLOE should be able to normalize the cross section for  $e^+e^- \rightarrow \pi^+\pi^-\gamma$  to that for  $e^+e^- \rightarrow \mu^+\mu^-\gamma$ . This is equivalent to measuring  $R$  in an energy scan and reduces the effects of theoretical systematics on the measurement. With  $2 \text{ fb}^{-1}$ , a  $\mu^+\mu^-\gamma$ -normalized measurement for  $\theta_\gamma > 40^\circ$  would allow the contribution to  $a_\mu^{\pi\pi}$  from the interval  $4m_\pi^2 < s < 0.9 \text{ GeV}^2$  to be determined with a statistical error of  $\sim 10 \times 10^{-11}$ .

In early 2006, KLOE also collected  $200 \text{ pb}^{-1}$  of data at  $\sqrt{s} = 1000 \text{ MeV}$ , at which  $\sigma(e^+e^- \rightarrow \phi \rightarrow \pi^+\pi^-\pi^0)$  drops to 5% of its peak value. These data will provide a better understanding of the background contributions, and, by themselves, should determine the contribution to  $a_\mu^{\pi\pi}$  as above, with a statistical error of  $\sim 35 \times 10^{-11}$  and greatly reduced systematic uncertainties.

## 6 THE DEAR AND SIDDHARTA EXPERIMENTS

### 6.1 Kaonic Atoms and the $\bar{K}N$ Interaction

In the language of chiral dynamics, the meson-nucleon “sigma terms,” which involve matrix elements of the form  $\langle N | m_q \bar{q}q | N \rangle$  ( $q \in u, d, s$ ), provide a measure of the effect of the scalar quark condensate on the nucleon, that is, the extent to which the chiral symmetry of QCD is broken. The values of the kaon-nucleon sigma terms are also directly related to the  $\bar{s}s$  content of the nucleon. The kaon-nucleon sigma terms are not experimentally observable, but can be obtained indirectly from measurements of the  $K^\pm N$  scattering amplitudes at threshold (i.e., scattering lengths) (123). Recently, interest in the  $\bar{K}N$  interaction has been fueled by the hypothesis that the interaction may be attractive enough to allow the formation of deeply bound  $\bar{K}$ -nuclear states (124), followed by claims of evidence for the existence of such states (see Section 7.2.2). Extrapolation of the existing  $K^-p$  scattering data to threshold and below is complicated by the presence of the  $\Lambda(1405)$ , as well as of open channels below threshold such as  $\bar{K}N \rightarrow Y\pi$  ( $Y = \Lambda, \Sigma$ ). Complementary information is available from the study of kaonic atoms.

A kaonic atom is formed when a  $K^-$  is captured in a high- $n$  electronic orbit of a normal atom. The kaon undergoes a cascade of transitions down to some final state of lower  $n$  and is then absorbed by the nucleus. The strong  $K^-N$  interaction causes the energy of this level to be shifted; the width of the spectral line is broadened by the absorption of the  $K^-$ . For a light system such as hydrogen, X-ray transitions to the  $n = 1$  level can be observed. The  $1s$  level shifts ( $\Delta_{1s}$ ) and widths ( $\Gamma_{1s}$ ) of the kaonic-hydrogen atom determine the isospin-averaged  $K^-p$  scattering length  $a_{K^-p}$  via the Deser relation (125).

For many years, kaonic-atom and scattering data seemed to give conflicting results. Various analyses of  $K^-p$  scattering data gave values for  $\Delta_{1s}$  and  $\Gamma_{1s}$  clustered around  $-360 \text{ eV}$  and  $510 \text{ eV}$ , respectively, indicating a repulsive interaction. The few existing measurements of the X-ray spectrum of kaonic hydrogen gave positive values for  $\Delta_{1s}$ , although the consistency of the results was poor. In 1997, a kaonic-hydrogen measurement from the KpX experiment at KEK was reported (126). The KpX values for  $\Delta_{1s}$  and  $\Gamma_{1s}$



are consistent with those from scattering data, but significantly less precise. The goal of the kaonic-atom program at DAΦNE is to measure  $\Delta_{1s}$  and  $\Gamma_{1s}$  at the level of a few eV.

## 6.2 Measurement of the X-Ray Spectrum of Kaonic Hydrogen

**6.2.1 DEAR** DEAR is literally a tabletop experiment. The apparatus shares the second DAΦNE interaction point with the FINUDA experiment—DEAR can be assembled when the FINUDA experiment is retracted.

Charged kaons from  $\phi$  decays at DAΦNE have kinetic energies of 16 MeV. The DEAR target cell is mounted approximately 10 cm above the beamline at the interaction point. Kaons traverse the thin-walled, aluminum/carbon-fiber beam pipe and kapton entrance window, are degraded to kinetic energies of a few MeV, and are stopped in the gaseous hydrogen (at temperature and pressure of 25 K and 2 bar, respectively) of the target cell. The target cell is 12.5 cm in diameter and 14 cm high and is constructed with low- $Z$  materials to avoid background from X-ray fluorescence in the energy region of interest. The hydrogen of the target is viewed by 16 charge-coupled device (CCD) detector chips with a total area of 116 cm<sup>2</sup>. The pixel size is  $22.5 \times 22.5 \mu\text{m}^2$ . The energy resolution of the CCD chips is 150 eV at 6 keV. In-beam energy calibration is obtained from the fluorescence lines from high- $Z$  foils deliberately placed in the target cell. The apparatus is further described in References 127 and 128.

After test runs and detector optimization during 2000–2001, DEAR took physics data in 2002. A first series of measurements with the target filled with nitrogen allowed machine-background studies, as well as an analysis of three transition lines in kaonic nitrogen (127). For the measurement with hydrogen (128),  $58.4 \text{ pb}^{-1}$  ( $\sim 90$  million  $K^-$ ) were collected. In general, soft (1–10 keV) X-rays deposit energy in one or two CCD pixels, whereas charged particles, higher-energy photons, and neutrons deposit energy in several adjacent pixels. The X-ray spectrum was therefore formed from single- and double-pixel events. In addition to the transition lines to be observed, the spectrum contains a continuous background component and fluorescence lines from detector materials. The background distribution was obtained from the analysis of runs taken with the beams separated at the interaction point, as well as of data from the nitrogen run. Parameters used in fits to the spectrum included the intensities of the hydrogen  $K_\alpha$  ( $2p \rightarrow 1s$ ),  $K_\beta$  ( $3p \rightarrow 1s$ ), and  $K_\gamma$  ( $4p \rightarrow 1s$ ) lines, the energy of the  $K_\alpha$  line, and one Lorentzian width for all  $K$  lines, as the hadronic broadening affects the  $1s$  level. The disentanglement of the  $K_\alpha$  lines from kaonic hydrogen and iron fluorescence, which partially overlap, required particular care.

Figure 16 shows a background-subtracted spectrum with the results of a fit superimposed. The complete analysis of the spectrum gives  $\Delta_{1s} = -193 \pm 37 \pm 6 \text{ eV}$  and  $\Gamma_{1s} = 249 \pm 111 \pm 30 \text{ eV}$ . These values are consistent with those from KpX, but with overall uncertainties that are lower by a factor of two. The absolute values of  $\Delta_{1s}$  and  $\Gamma_{1s}$  from DEAR are  $\sim 50\%$  lower than those derived from  $K^-p$  scattering data.

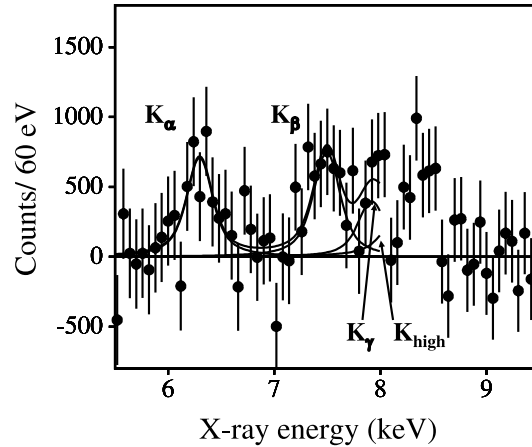


**Fig. 16.** Background-subtracted X-ray spectrum for kaonic hydrogen from DEAR, with fit to  $K$ -series spectral lines.

**6.2.2 INTERPRETATION** The  $K^-p$  interaction appears to be repulsive from kaonic-hydrogen and scattering data. If the  $\Lambda(1405)$  is interpreted as an  $I = 0$   $K^-p$  bound state just below threshold, scattering through this resonance gives rise to a repulsive contribution to the scattering length. A systematic study of heavy-kaonic-atom data suggests that the  $K^-$ -nuclear optical potential is strongly attractive in the nuclear interior (129), which may be explained by the dissolution of the  $\Lambda(1405)$  (130). Detailed calculations give variable results for the optical potential (131). If the  $\bar{K}N$  attraction in medium is strong enough to close the decay channel to  $\Sigma\pi$ ,  $\bar{K}$ -nuclear states with binding energies of  $\sim 100$  MeV and widths of a few tens of MeV may be formed (124), although this scenario is not universally accepted (132). Systematic analyses of the  $\bar{K}N$  interaction in the near-threshold region may help to establish or disprove this scenario; the DEAR measurement of the  $K^-p$  scattering length provides an important constraint in such analyses (see, e.g., Reference 133). However, the origin of the inconsistency between the DEAR results and the data from  $K^-p$  scattering requires clarification.

**6.2.3 FUTURE DIRECTIONS: SIDDHARTA** The program of kaonic-atom measurements at DAΦNE will be continued using the SIDDHARTA (Silicon Drift Detector for Hadronic Atom Research by Timing Applications) apparatus (135). Improvements on the precision of the DEAR measurement require a substantial reduction in machine-background levels. The machine background in DEAR is primarily from beam particles lost to intrabunch scattering or beam-gas interactions. Effective background suppression can be obtained from timing measurements, e.g., by requiring the coincidence between  $K^+$  and  $K^-$  signals in a scintillator telescope together with the signal from the detector. The DEAR CCDs are read out once every 90 s, so the use of timing information is not possible. In contrast, it is possible with an instrument based on an array of silicon drift detectors. Silicon drift detectors are low-noise devices; the expected energy resolution is comparable to or better than that of the DEAR CCDs. The SIDDHARTA detector will be ready to take data during the 2007 DAΦNE run. The planned experimental program includes (a) the collection of  $500 \text{ pb}^{-1}$  of hydrogen data for the measurement of  $\Delta_{1s}$  and  $\Gamma_{1s}$  with electron-volt precision, (b)  $1000 \text{ pb}^{-1}$  of deuterium data to allow separate determination of the  $I = 0$  and  $I = 1$   $\bar{K}N$  scattering lengths, and (c) a shorter run with helium that may offer evidence in favor of deeply bound  $K^-^3\text{He}$  states (136), if they exist.

## 7 FINUDA

### 7.1 Hypernuclear Physics at a $\phi$ Factory

A hypernucleus is formed when one or more nucleons in a conventional nucleus are replaced by hyperons (most commonly  $\Lambda$ s). The hyperon ( $Y$ ) is distinguished from the other nucleons by its strangeness quantum number and is not subject to the Pauli exclusion principle. It can therefore occupy any nuclear level. The hypernuclear level structure provides valuable information about the  $YN$  interaction. Hypernuclei with  $A > 5$  decay principally via the nonmesonic channels  ${}^A_\Lambda Z \rightarrow {}^{A-2}Z nn$  and  ${}^A_\Lambda Z \rightarrow {}^{A-2}(Z-1)np$ , where the underlying process is  $\Lambda N \rightarrow NN$ . Thus, the decays of hypernuclei also offer information about the weak interaction between baryons (see Reference 137 for a review).

FINUDA is a fixed-target experiment at an  $e^+e^-$  collider. Hypernuclei are formed when  $K^-$ s from  $\phi$  decays are stopped in targets surrounding the beam pipe and interact via  $K^-_{\text{stop}} {}^A Z \rightarrow {}^A_\Lambda Z \pi^-$ . The spectrum of hypernuclear levels is obtained from the momentum distribution of the  $\pi^-$  emitted when the hypernucleus is formed at rest. In addition, hypernuclear decays can be studied by reconstructing the charged decay products ( $\pi^-$ ,  $p$ ,  $d$ ). The low energy of the  $K^-$  “beam” ( $E_{\text{kin}} = 16$  MeV) allows targets as thin as  $0.2 \text{ g/cm}^2$  to be used, so that the intrinsic momentum resolution of the spectrometer can be fully exploited. FINUDA covers a solid angle of  $\sim 2\pi$ . Because of the large acceptance of the detector,  $\sim 80$  hypernuclei/hour can be observed at a luminosity of  $10^{32} \text{ cm}^{-2} \text{ s}^{-1}$ , assuming a capture rate of  $10^{-3}$ .

The FINUDA detector is illustrated in Figure 17. The detector is subdivided into three concentric cylindrical regions: an interaction/target region, an external tracking region, and an outer TOF barrel. A superconducting solenoid 1.5 m in radius and 2.1 m in length surrounds the entire experiment and provides a 1 T magnetic field.

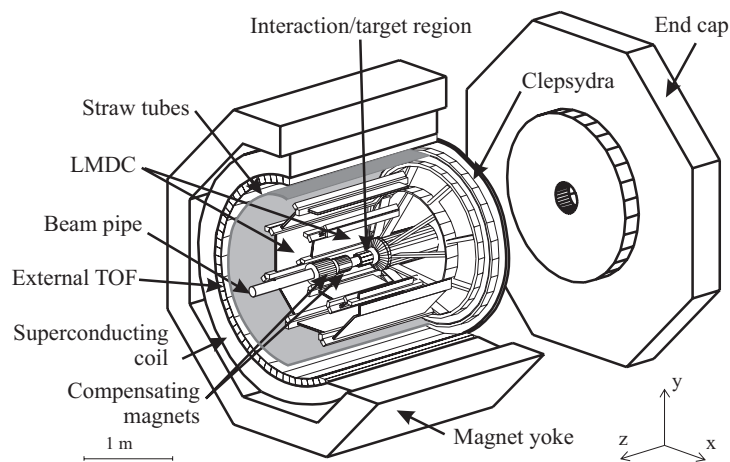


**Fig. 17.** Diagram of the FINUDA experiment.

Kaons from  $\phi$  decays at the interaction point traverse the beryllium beam pipe and enter the interaction/target region. Before encountering one of the eight solid targets arranged in an octagonal array about the beam pipe, they cross an inner TOF barrel (time resolution of  $\sigma_t = 250$  ps), which is used for trigger definition, and a layer of double-sided silicon-microstrip detectors (spatial resolution of  $\sigma = 30 \mu\text{m}$ ), which are used to reconstruct the interaction positions in the targets. The secondaries emerge into the external tracking region, which contains four concentric detector systems: a second layer of silicon

microstrips; two cylindrical arrays of planar, low-mass DCs; and a straw-tube detector consisting of six layers of longitudinal and stereo tubes. The external tracking region is filled with helium to minimize the effects of multiple scattering. The design momentum resolution of the tracking system for a  $\pi^-$  with  $p = 270$  MeV (typical of hypernuclear formation) is 0.8 MeV FWHM, which determines the limiting energy resolution for hypernuclear levels. The external TOF barrel consists of 72 10-cm-thick scintillator slabs. The time resolution is 350 ps; the detection efficiency for neutrons from hypernuclear decay is 10%. More information about the FINUDA detector is available in References 138 and 139.

FINUDA first took data between October 2003 and March 2004.  $50 \text{ pb}^{-1}$  were collected for machine studies and detector calibration;  $200 \text{ pb}^{-1}$  were collected for analysis. The eight targets used were  ${}^6\text{Li}$  (isotopically enriched, two targets),  ${}^7\text{Li}$ ,  ${}^{12}\text{C}$  (three targets),  ${}^{27}\text{Al}$ , and  ${}^{51}\text{V}$ . Much data exist on  ${}^1_0\text{C}$ ; the three  ${}^{12}\text{C}$  targets were included principally to provide calibration for the experiment's maiden run. Using these targets, FINUDA has obtained a precise measurement of the  ${}^{12}_\Lambda\text{C}$  excitation spectrum (Section 7.2.1). The  ${}^6\text{Li}$  and  ${}^7\text{Li}$  targets allow FINUDA to observe the nonmesonic decays of light hypernuclei. The light targets ( ${}^6\text{Li}$ ,  ${}^7\text{Li}$ , and  ${}^{12}\text{C}$ ) can also be used to search for neutron-rich hypernuclei (140) and deeply bound  $\bar{K}$ -nuclear states (Section 7.2.2). Using the heavier targets, FINUDA should improve significantly on the current precision of the excitation spectra for  ${}^{27}_\Lambda\text{Al}$  and  ${}^{51}_\Lambda\text{V}$ , as well as measure the ground-state capture rates.

## 7.2 First Results from the FINUDA Experiment

**7.2.1 REACTION SPECTRUM OF  ${}^{12}_\Lambda\text{C}$**  The FINUDA measurement of the reaction spectrum of  ${}^{12}_\Lambda\text{C}$  (139) demonstrates the potential of the experiment for hypernuclear spectroscopy. Candidate hypernuclear events were identified by the simultaneous presence of  $dE/dx$ -identified  $K^+$  and  $K^-$  hits in the inner detectors, together with a high-quality track corresponding to the  $\pi^-$  in the outer detectors.

The binding-energy spectrum of  ${}^{12}_\Lambda\text{C}$  shown in Figure 18 (left panel) is obtained from the distribution of the  $\pi^-$  momentum.

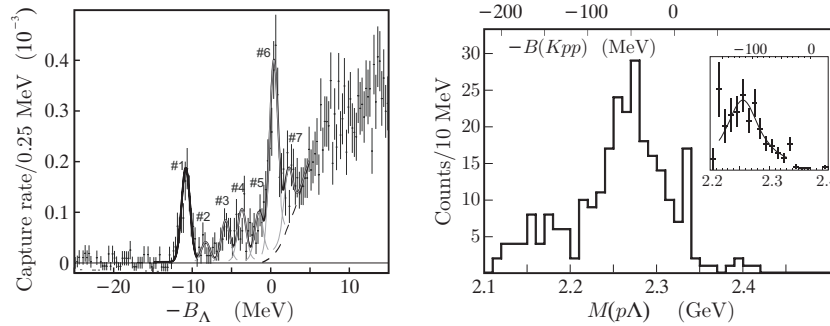


**Fig. 18.** (Left panel) Binding-energy spectrum for  ${}^{12}_\Lambda\text{C}$  with fit to peaks plus quasi-free background (dashed line). (Right panel)  $M_{\Lambda p}$  spectrum for events from light targets with  $\cos\theta_{\Lambda p} < -0.8$ . (Right panel inset) Peak after acceptance corrections. From FINUDA.

The two prominent peaks at  $B_\Lambda \approx 11$  MeV (#1 in Figure 18) and  $B_\Lambda \approx 0$  MeV (#6) correspond to the ground-state configuration with the  $\Lambda$  in the  $s$  shell and to the excited state with the  $\Lambda$  in the  $p$  shell, respectively. The measured value of the capture rate for the ground state is  $(1.01 \pm 0.11 \pm 0.10) \times 10^{-3}$  per stopped  $K^-$ . By fitting the ground-state peak

with a Gaussian, the energy resolution was determined to be 1.29 MeV FWHM. These results were obtained without the detector fully calibrated; the momentum resolution may be improved in future analyses. FINUDA has also performed different fits to the entire spectrum. The fit shown in Figure 18 was to seven Gaussian peaks with free central values and weights;  $\sigma$  for all peaks was fixed to 0.55 MeV. The fit also included the quasi-free component illustrated as the dashed line.

The  $^{12}_\Lambda\text{C}$  reaction spectrum was previously measured by the E369 experiment at KEK (141), in which hypernuclei were produced from a  $\pi^+$  beam by associated production ( $\pi^+ {}^A_Z \rightarrow {}^A_\Lambda Z K^+$ ). The energy resolution was 1.45 MeV FWHM. FINUDA compares the positions and strengths of the peaks in Figure 18 (left panel) to those seen in the E369 data. The momentum transfer to the  $\Lambda$  in E369 is  $\sim 350$  MeV, as compared with  $\sim 250$  MeV in FINUDA. As a result, the relative weights observed for the  $s_\Lambda$  and  $p_\Lambda$  peaks are expected to differ (142). Some differences are also noted in the structure around peaks #3, #4, and #5. Several excited states of the  $^{11}\text{C}$  core nucleus may contribute to the structure in this energy region (143).

FINUDA uses the ground-state peak to normalize the capture rates for the other peaks and compares the resulting values to older data on  $^{12}_\Lambda\text{C}$  from stopped  $K^-$  experiments and to the results of various calculations. In general, the capture rates for the identified peaks in the FINUDA spectrum are significantly larger than calculations predict, whereas the FINUDA capture rates for the stronger peaks observed in older experiments are in reasonable agreement with the older results.

**7.2.2 NEW STATES FROM NUCLEAR  $K^-$  ABSORPTION AT REST** The E471 group at KEK claims to have observed two  $S = -1$  tribaryon states from  $K^-$  capture at rest:  $K^-_{\text{stop}} {}^4\text{He} \rightarrow XN_r$ , where the recoil nucleon  $N_r$  is  $p$  or  $n$  (144). The states are seen as peaks in the missing-mass distributions as reconstructed from the TOF-measured velocity of the recoil nucleon. A peak with a significance of  $8.2\sigma$  in the distribution for events with a recoil proton is interpreted to be from the reaction  $K^- (pnn) \rightarrow S^0 \rightarrow \Sigma NN$  or  $\Sigma^- d$ . The  $S^0(3115)$  is an isospin triplet state with an excitation energy of  $\sim 44$  MeV and a width of  $< 22$  MeV. For events with a recoil neutron, a  $3.7\sigma$  peak is observed and attributed to  $K^- (ppn) \rightarrow S^+ \rightarrow \Sigma^+ nn$  or  $\Sigma^- pp$ . The  $S^+(3140)$  is an isospin singlet with an excitation energy of  $\sim 69$  MeV and a width of  $< 22$  MeV. If interpreted as  $K^- NNN$  bound states (see Section 6.2.2), the  $S^0$  and  $S^+$  have binding energies of 194 MeV and 169 MeV. The nonrelativistic calculations of Reference 124 do not predict the existence of the  $S^0$ ; they find a state similar to the  $S^+$ , but of higher mass. Such calculations are questionable. An alternative explanation of the data in which the peaks correspond to the process  $K^- NN \rightarrow YN$  (with the remaining two nucleons spectators) has also been proposed (132).

While the E471 results are based only on TOF measurements, FINUDA can reconstruct the charged particles in the final state and compute invariant masses. FINUDA has studied the  $\Lambda p$  invariant-mass distribution following  $K^-$  capture in the light targets ( ${}^6\text{Li}$ ,  ${}^7\text{Li}$ , and  $^{12}\text{C}$ ) (145). For a normal two-nucleon absorption process,  $M_{\Lambda p}$  should peak sharply at  $\sim 30$  MeV below  $m_{K^-} + 2m_p$ . Instead, the  $M_{\Lambda p}$  distribution for events with  $\cos \theta_{\Lambda p} < -0.8$  is broadly peaked, as shown in Figure 18 (right panel). A fit gives a mass of  $2255^{+5}_{-6}$  MeV and a width of  $67^{+14}_{-11}$  MeV. FINUDA attributes this peak to the decay of a  $K^- pp$  bound state, in which case the binding energy is 115 MeV. The  $\Lambda p$  excitation energy is 201 MeV, which is large and consistent with the large width. Especially in light nuclei, two-nucleon absorption followed by rescattering effects could give rise to a peak like that observed (146). We are skeptical of the need to invoke deeply bound  $\bar{K}$ -nuclear or multiquark states to explain the peaks observed by E471 and FINUDA.

FINUDA will resume data taking during summer 2006 and expects to collect  $1 \text{ fb}^{-1}$ . The planned target set includes light targets such as  ${}^6\text{Li}$  and  ${}^9\text{Be}$ , which are nearly  $\alpha d$  and  $\alpha n$  clusters, and are ideal for use in the search for new states.

## 8 THE FUTURE OF DAΦNE

KLOE finished taking data at  $\sqrt{s} = m_\phi$  in December 2005 and collected a small amount of off-peak data necessary to round out the data set in January–March 2006. During the latter half of 2006, DAΦNE running will be dedicated to FINUDA; SIDDHARTA will run in 2007. Thus the original DAΦNE program will be completed, except for the search for direct  $CP$  violation.

Discussion concerning what sort of facility may replace DAΦNE began formally at Alghero in September 2003 (147). Many options have been considered (148). One likely alternative is a second-generation DAΦNE, with a luminosity increased by a factor of  $\sim 5$  at  $\sqrt{s} = m_\phi$ , possibly capable of running at energies up to the  $N\bar{N}$  threshold. However, a definite proposal will probably not emerge until late 2006.

Meanwhile, the KLOE study of leptonic and semileptonic kaon decays has been extremely successful. Using  $\sim 1/5$  of the available data, KLOE has measured  $f_+^{K^0}(0)|V_{us}| = 0.2167 \pm 0.0005$ , i.e., with an accuracy of  $\pm 0.23\%$ , from which  $|V_{us}| = 0.2255 \pm 0.0019$  and  $|V_{ud}|^2 + |V_{us}|^2 + |V_{ub}|^2 = 0.9991 \pm 0.0010$ . The error is dominated by theoretical uncertainties on  $f_+^{K^0}(0)$  that will likely decrease in the near future. These results establish that it is possible to reach accuracies below 0.1%.

The decay-rate measurements discussed provide access to a series of effective couplings, such as  $G_e$ ,  $G_\mu$ ,  $G_q|V_{ud}|$ , and  $G_q|V_{us}|$ . If there is new physics at the TeV scale, it will be reflected in the values of these effective couplings. Lepton universality is the statement that  $G_e = G_\mu \cdots = G_\ell$ . Unitarity in the quark sector refers to the CKM matrix; in addition, the full Standard Model requires  $G_\ell = G_q = G_F$ . New physics may change this simple picture at the level of 0.1%. In testing universality, if we limit ourselves to  $e$ ,  $\mu$ ,  $u$ ,  $d$ , and  $s$ , we have five parameters and need five measurements. Kaons provide three:  $\Gamma(K_{\ell 3})$ ,  $\Gamma(K_{\mu 2})$ , and  $\Gamma(K_{e 2})$ . With the addition of the muon and pion lifetimes, we have five. The half-lives for  $0^+ \rightarrow 0^+$  nuclear  $\beta$ -transitions provide a welcome check. We consider these measurements central to the future of a  $\phi$  factory.

## Acknowledgements

We would like to thank our fellow KLOE collaborators for their heroic dedication and brilliance in bringing about “questa bella e grande avventura.” We would also like to warmly congratulate the members of the DAΦNE staff and of the DEAR and FINUDA Collaborations on their achievements. Finally, we thank Juliet Lee-Franzini for a critical reading of this manuscript.

## LITERATURE CITED

1. Christenson JH, Cronin JW, Fitch VL, Turlay R. *Phys. Rev. Lett.* 13:138 (1964)
2. Wolfenstein L. *Phys. Rev. Lett.* 13:562 (1964)
3. Burkhardt H, et al. (NA31 Collab.) *Phys. Lett. B* 206:169 (1988); Patterson JR, et al. *Phys. Rev. Lett.* 64:1491 (1990)
4. Document number LNF-90/031(R). Lab. Naz. Frascati (1990).  
<http://www.lnf.infn.it/sis/preprint>



5. Aloisio A, et al. (KLOE Collab.) Document number LNF-92/019(IR). Lab. Naz. Frascati (1992). <http://www.lnf.infn.it/sis/preprint>
6. Agnello M, et al. (FINUDA Collab.) Document number LNF-93/021(IR). Lab. Naz. Frascati (1993). <http://www.lnf.infn.it/sis/preprint>
7. Baldini R, et al. (DEAR Collab.) Document number LNF-95/055(IR). Lab. Naz. Frascati (1995). <http://www.lnf.infn.it/sis/preprint>
8. Bassetti M, et al. DAΦNE Intern. Tech. Note L-1. Lab. Naz. Frascati (1991). <http://www.lnf.infn.it/acceleratori/dafne/technotes.html>
9. Zobov M. (DAΦNE Collab.) *Proc. Eur. Part. Accel. Conf., Vienna, 2000*. Geneva: CERN (2000). <http://accelconf.web.cern.ch>
10. Adinolfi M, et al. *Nucl. Instrum. Methods A* 488:51 (2002)
11. Adinolfi M, et al. *Nucl. Instrum. Methods A* 482:364 (2002)
12. Adinolfi M, et al. *Nucl. Instrum. Methods A* 483:649 (2002)
13. Adinolfi M, et al. *Nucl. Instrum. Methods A* 492:134 (2002)
14. Aloisio A, et al. *Nucl. Instrum. Methods A* 516:288 (2004)
15. Ambrosino F, et al. *Nucl. Instrum. Methods A* 534:403 (2004)
16. Duniety I, Hauser J, Rosner JL. *Phys. Rev. D* 35:2166 (1987)
17. Pancheri G, ed. *Proc. Workshop Phys. Detect. DAΦNE, Frascati, 1991*. Frascati, Italy: Lab. Naz. Frascati (1991)
18. Franzini P. See Ref. 17, p. 733 (1991)
19. Buchanan CD, et al. *Phys. Rev. D* 45:4088 (1992)
20. Maiani L, Pancheri G, Paver N, eds. *The Second DAΦNE Physics Handbook*, Frascati, Italy: Lab. Naz. Frascati (1995)
21. D'Ambrosio G, Isidori G, Pugliese A. See Ref. 20, p. 63 (1995)
22. *Proc. Int. Europhys. Conf. High Energy Phys. (HEP2005), Lisbon, 2005*, Trieste, Italy: Sc. Int. Super. Stud. Avanzati (2006). <http://pos.sissa.it>
23. Moulson M. (KLOE Collab.) See Ref. 22, PoS(HEP2005)264 (2006)
24. Batley JR, et al. *Phys. Lett. B* 544:97 (2002)
25. Alavi-Harati A, et al. (KTeV Collab.) *Phys. Rev. D* 67:012005 (2003)
26. Kobayashi M, Maskawa T. *Prog. Theor. Phys.* 49:652 (1973)
27. Cabibbo N. *Phys. Rev. Lett.* 10:531 (1963)
28. Sher A, et al. *Phys. Rev. Lett.* 91:261802 (2003)
29. Alexopoulos T, et al. (KTeV Collab.) *Phys. Rev. Lett.* 93:181802 (2004); Alexopoulos T, et al. *Phys. Rev. D* 70:092006 (2004)
30. Alexopoulos T, et al. (KTeV Collab.) *Phys. Rev. D* 70:092007 (2004)
31. Yushchenko OP, et al. *Phys. Lett. B* 589:111 (2004)
32. Yushchenko OP, et al. *Phys. Lett. B* 581:31 (2004)
33. Lai A, et al. (NA48 Collab.) *Phys. Lett. B* 604:1 (2004)
34. Chen H, Du D, Li W, Lu C, eds. *Proc. Int. Conf. High Energy Phys. (ICHEP), 32nd, Beijing, 2004*, Singapore: World Sci. (2005)
35. Litov L. (NA48 Collab.) See Ref. 34, p. 817 (2005)
36. Lai A, et al. (NA48 Collab.) *Phys. Lett. B* 602:41 (2004)
37. Gatti C. *Eur. Phys. J. C* 45:417 (2006)
38. Ademollo M, Gatto R. *Phys. Rev. Lett.* 13:264 (1964)
39. Sirlin A, *Rev. Mod. Phys.* 50:573 (1978); *Nucl. Phys. B* 196:83 (1982)
40. Cirigliano V, et al. *Eur. Phys. J. C* 23:121 (2002); Cirigliano V, Neufeld H, Pichl H. *Eur. Phys. J. C* 35:53 (2004)
41. Davies CTH, et al. *Phys. Rev. Lett.* 92:022001 (2004)
42. Marciano WJ, *Phys. Rev. Lett.* 93:231803 (2004)
43. Finkemeier M. *Phys. Lett. B* 387:391 (1996); Finkemeier M. See Ref. 20, p. 389



- (1995); Decker R, Finkemeier M. *Phys. Lett. B* 334:199 (1994)
44. *Proc. Int. Symp. Lattice Field Theory, 23rd, Dublin, 2005*, Trieste, Italy: Sc. Int. Super. Stud. Avanzati (2005). <http://pos.sissa.it>
  45. Bernard C, et al. See Ref. 44, PoS(LAT2005)025 (2005)
  46. Ambrosino F, et al. (KLOE Collab.) *Phys. Lett. B* 608:199 (2005);
  47. Antonelli M, Dreucci M. KLOE Note 181. Lab. Naz. Frascati (2002). <http://www.lnf.infn.it/kloe/kn181.ps>
  48. Akhmetshin RR, et al. *Phys. Lett. B* 466:385 (1999); Erratum. *Phys. Lett. B* 508:217 (2001)
  49. Ambrosino F, et al. (KLOE Collab.) *Phys. Lett. B* 626:15 (2005)
  50. Vosburgh KG, et al., *Phys. Rev. D* 6:1834 (1972)
  51. Ambrosino F, et al. (KLOE Collab.) *Phys. Lett. B* 632:43 (2006)
  52. Eidelman S, et al. (Part. Data Group) *Phys. Lett. B* 592:1 and web updates, <http://pdg.lbl.gov> (2004)
  53. Bijnens J, Borg F. *Eur. Phys. J. C* 40:383 (2005)
  54. Ambrosino F, et al. (KLOE Collab.) *Phys. Lett. B* 636:166 (2006)
  55. Spadaro T. (KLOE Collab.) *Proc. Int. Conf. Calorim. Part. Phys., 11th, Perugia, 2004*, p. 337. Singapore: World Sci. (2005)
  56. Cirigliano V, Ecker G, Neufeld H, Pich A. *Eur. Phys. J. C* 33:369 (2004)
  57. Aloisio A, et al. (KLOE Collab.) *Phys. Lett. B* 538:21 (2002)
  58. Ambrosino F, et al. (KLOE Collab.) *Eur. Phys. J. C* hep-ex/0601025. In press
  59. Alavi-Harati A, et al. (KTeV Collab.) *Phys. Rev. Lett.* 88:181601 (2002)
  60. Angelopoulos A, et al. (CLEAR Collab.) *Phys. Lett. B* 444:52 (1998)
  61. Apostolakis A, et al. (CLEAR Collab.) *Phys. Lett. B* 456:297 (1999)
  62. Angelopoulos A, et al. (CLEAR Collab.) *Phys. Lett. B* 444:38 (1998)
  63. Aloisio A, et al. (KLOE Collab.) *Phys. Lett. B* 535:37 (2002)
  64. Ambrosino F, et al. (KLOE Collab.) *Phys. Lett. B* 636:173 (2006)
  65. Ambrosino F, et al. (KLOE Collab.) *Phys. Lett. B* 619:61 (2005)
  66. Lai A, et al. (NA48 Collab.) *Phys. Lett. B* 610:165 (2005)
  67. Chiang IH, et al. *Phys. Rev. D* 6:1254 (1972)
  68. Ott RJ, Pritchard TW. *Phys. Rev. D* 3:52 (1971)
  69. Ambrosino F, et al. (KLOE Collab.) *Phys. Lett. B* 632:76 (2006)
  70. Sciascia B. (KLOE Collab.) See Ref. 22, PoS(HEP2005)287 (2006)
  71. Leutwyler H, Roos M. *Z. Phys. C* 25:91 (1984)
  72. Bećirević D, et al. *Nucl. Phys. B* 705:339 (2005); Dawson C, et al. (RBC Collab.) See Ref. 44, PoS(LAT2005)337 (2005)
  73. Marciano WJ, Sirlin A. *Phys. Rev. Lett.* 96:032002 (2006)
  74. Lai A, et al. *Phys. Lett. B* 533:196 (2002)
  75. Abdel-Bary M, et al. (GEM Collab.) *Phys. Lett. B* 619:281 (2005)
  76. Bijnens J, Galt G, Nefkens BMK, eds. *Eta Phys. Handb.: Proc. Workshop Eta Phys., Uppsala, 2001. Phys. Scripta* T99 (2002)
  77. Holstein BR. See Ref. 76, p. 55 (2002)
  78. Bijnens J, Gasser J. See Ref. 76, p. 34 (2002)
  79. Tippens WB, et al. (Cryst. Ball Collab.) *Phys. Rev. Lett.* 87:192001 (2001)
  80. Ametller Ll, Bijnens J, Bramon A, Cornet F. *Phys. Lett. B* 276:185 (1992)
  81. Alde D, et al. *Z. Phys. C* 25:225 (1984)
  82. Prakhov S, et al. (Cryst. Ball Collab.) *Phys. Rev. C* 72:025201 (2005)
  83. Bijnens J, Fayyazuddin A, Prades J. *Phys. Lett. B* 379:209 (1996)
  84. Bel'kov AA, Lanyov AV, Scherer S. *J. Phys. G* 22:1383 (1996)
  85. Aloisio A, et al. (KLOE Collab.) *Phys. Lett. B* 591:49 (2004)

86. Ambrosino F, et al. (KLOE Collab.) *Phys. Lett. B* 606:276 (2005)
87. Rosner JL. *Phys. Rev. D* 27:1101 (1983)
88. Feldmann Th. *Int. J. Mod. Phys. A* 15:159 (2000)
89. Aloisio A, et al. (KLOE Collab.) *Phys. Lett. B* 541:45 (2002)
90. Bramon A, Escribano R, Scadron MD. *Eur. Phys. J. C* 7:271 (1999)
91. Jaffe, RL. *Phys. Rev. D* 15:267 (1977); Alford M, Jaffe RL. *Nucl. Phys. B* 578:367 (2000)
92. Weinstein J, Isgur N. *Phys. Rev. Lett.* 48:659 (1982)
93. Törnqvist, NA. *Z. Phys. C* 68:647 (1995)
94. Boglione M, Pennington MR. *Phys. Rev. D* 65:114010 (2002)
95. Achasov NN, Ivanchenko VN. *Nucl. Phys. B* 315:465 (1989)
96. Achasov NN, Gubin VV. *Phys. Rev. D* 56:4084 (1997)
97. Kalashnikova YuS, et al. *Eur. Phys. J. A* 24:437 (2005)
98. Aloisio A, et al. (KLOE Collab.) *Phys. Lett. B* 537:21 (2002)
99. Aloisio A, et al. (KLOE Collab.) *Phys. Lett. B* 536:209 (2002)
100. Akhmetshin RR, et al. *Phys. Lett. B* 462:380 (1999)
101. Achasov MN, et al. *Phys. Lett. B* 485:349 (2000)
102. Achasov MN, et al. *Phys. Lett. B* 479:53 (2000)
103. Close FE, Törnqvist NA. *J. Phys. G* 28:R249 (2002)
104. Achasov NN, Kiselev AV. *Phys. Rev. D* 68:014006 (2003)
105. Oller JA. *Nucl. Phys. A* 714:161 (2003)
106. Achasov NN, Kiselev AV. *Phys. Rev. D* 73:054029 (2006)
107. Boglione M, Pennington MR. *Eur. Phys. J. C* 30:503 (2003)
108. Isidori G, Maiani L, Nicolaci M, Pacetti S. *JHEP* 0605:049 (2006)
109. Flatté SM. *Phys. Lett. B* 63:224 (1976)
110. Ambrosino F, et al. (KLOE Collab.) *Phys. Lett. B* 634:148 (2006)
111. Achasov NN, Gubin VV. *Phys. Rev. D* 57:1987 (1998)
112. Bennett GW, et al. (Muon  $g - 2$  Collab.) *Phys. Rev. Lett.* 92:161802 (2004)
113. Akhmetshin RR, et al. *Phys. Lett. B* 578:285 (2004)
114. Davier M, Marciano WJ. *Annu. Rev. Nucl. Part. Sci.* 54:115 (2004)
115. Davier M, Eidelman S, Höcker A, Zhang Z. *Eur. Phys. J. C* 31:503 (2003)
116. Czyż H, Grzelińska A, Kühn JH, Rodrigo G. *Eur. Phys. J. C* 33:333 (2004)
117. Binner S, Kühn JH, Melnikov K. *Phys. Lett. B* 459:279 (1999)
118. Aloisio A, et al. (KLOE Collab.) *Phys. Lett. B* 606:12 (2005)
119. Höcker A. See Ref. [34](#), p. 710 (2005)
120. Achasov MN, et al. *J. Exp. Theor. Phys.* 101:1053 (2005)
121. Davier M, Höcker A, Zhang Z. *Rev. Mod. Phys.* hep-ex/0507078. In press
122. Sibidanov AL. (CMD-2 Collab.) *Proc. Int. Conf. Hadron Spectrosc. (HADRON), 11th, Rio de Janeiro, 2005*, p. 478. Melville, NY: Am. Inst. Phys. (2006)
123. Gasser J, Sainio ME. *Proc. Int. Workshop Phys. Detect. DAΦNE, 3rd, Frascati, 1999*, p. 659. Frascati, Italy: Lab. Naz. Frascati (1999)
124. Akaishi Y, Yamazaki T. *Phys. Rev. C* 65:044005 (2002)
125. Deser S, Goldberger ML, Baumann K, Thirring W. *Phys. Rev.* 96:774 (1954)
126. Iwasaki M, et al. *Phys. Rev. Lett.* 78:3067 (1997)
127. Ishiwatari T, et al. *Phys. Lett. B* 593:48 (2004)
128. Beer G, et al. (DEAR Collab.) *Phys. Rev. Lett.* 94:212302 (2005)
129. Friedman E, Gal A, Batty CJ. *Nucl. Phys. A* 579:518 (1994)
130. Koch V. *Phys. Lett. B* 337:7 (1994)
131. Waas T, Kaiser N, Weise W. *Phys. Lett. B* 365:12 (1996); Ramos A, Oset E. *Nucl. Phys. A* 671:481 (2000)

- 132. Oset E, Toki H. nucl-th/0509048
- 133. Borasoy B, Nißler R, Weise W. *Eur. Phys. J. A* 25:79 (2005)
- 134. Hirtl A, Marton J, Widmann E, Zmeskal J, eds. *Proc. Int. Conf. Exot. At. Relat. Top. (EXA05), Vienna, 2005*, Vienna: Austrian Acad. Sci. (2005)
- 135. Zmeskal J. (DEAR and SIDDHARTA Collab.) See Ref. 134, p. 139 (2005)
- 136. Akaishi Y. See Ref. 134, p. 45 (2005)
- 137. Alberico WM, Garbarino G. *Phys. Rep.* 369:1 (2002)
- 138. Agnello M, et al. (FINUDA Collab.) Document number LNF-95/024(IR). Lab. Naz. Frascati (1995). <http://www.lnf.infn.it/sis/preprint>
- 139. Agnello M, et al. (FINUDA Collab.) *Phys. Lett. B* 622:35 (2005)
- 140. Agnello M, et al. (FINUDA Collab.) . *Proc. Int. Conf. DAΦNE 2004: Phys. Meson Factories, Frascati, 2004*, p. 201. Frascati, Italy: Lab. Naz. Frascati (2004)
- 141. Hotchi H, et al. *Phys. Rev. C* 64:044302 (2001)
- 142. Itonaga K, Motoba T, Bandō H. *Prog. Theor. Phys.* 84:291 (1990)
- 143. Motoba T. *Proc. Int. Conf. Hypernucl. Strange Part. Phys., 6th (HYP97), Upton, New York, 1997. Nucl. Phys. A* 639:135c (1998)
- 144. Suzuki T, et al. *Proc. Int. Conf. Hypernucl. Strange Part. Phys., 8th (HYP2003), Newport News, Virginia, 2003. Nucl. Phys. A* 754:375c (2005)
- 145. Agnello M, et al. (FINUDA Collab.) *Phys. Rev. Lett.* 94:212303 (2005)
- 146. Magas VK, Oset E, Ramos A, Toki H. nucl-th/0601013 (2006)
- 147. Biscari C, Bossi F, Isidori G, eds. *Proc. Workshop  $e^+e^-$  1–2 GeV Range: Phys. Accel. Prospects, Alghero, 2003*. eConf C0309101 (2003). <http://www.lnf.infn.it/conference/d2>
- 148. Benfatto M, et al., eds. Document number LNF-05/033(IR). Lab. Naz. Frascati (2005). <http://www.lnf.infn.it/sis/preprint>